

Weakly nonlinear analysis of a hyperbolic model for animal group formation

R. Eftimie · G. de Vries · M. A. Lewis

Received: 12 December 2007 / Revised: 3 June 2008 / Published online: 3 September 2008
© Springer-Verlag 2008

Abstract We consider an one-dimensional nonlocal hyperbolic model for group formation with application to self-organizing collectives of animals in homogeneous environments. Previous studies have shown that this model displays at least four complex spatial and spatiotemporal group patterns. Here, we use weakly nonlinear analysis to better understand the mechanisms involved in the formation of two of these patterns, namely stationary pulses and traveling trains. We show that both patterns arise through subcritical bifurcations from spatially homogeneous steady states. We then use these results to investigate the effect of two social interactions (attraction and alignment) on the structure of stationary and moving animal groups. While attraction makes the groups more compact, alignment has a dual effect, depending on whether the groups are stationary or moving. More precisely, increasing alignment makes the stationary groups compact, and the moving groups more elongated. Also, the results show the existence of a threshold for the total group density, above which, coordinated behaviors described by stationary and moving groups persist for a long time.

R. Eftimie (✉) · G. de Vries · M. A. Lewis
Department of Mathematical and Statistical Sciences, University of Alberta,
Edmonton, AB T6G 1H7, Canada
e-mail: reftimie@math.ualberta.ca

Present Address:

R. Eftimie
Department of Mathematics and Statistics, McMaster University,
Hamilton, ON L8S 4L8, Canada
e-mail: reftimie@math.mcmaster.ca

M. A. Lewis
Department of Biological Sciences, University of Alberta,
Edmonton, AB T6G 2E9, Canada

Keywords Nonlocal hyperbolic system · Animal group formation · Weakly nonlinear analysis

Mathematics Subject Classification (2000) Primary 92B05; Secondary 35L60 · 37G99

1 Introduction

The study of animal aggregations (such as schools of fish, swarms of insects, etc.) has become a topic of recent interest [15, 19, 31, 35, 40]. One of the most studied aspects of these aggregations is the spatial and spatiotemporal patterns they form. Examples of such patterns range from stationary aggregations formed by resting animals, to zigzagging flocks of birds or milling schools of fish. To gain insight into how different mechanisms influence pattern formation, scientists use mathematical models motivated by biologically based hypotheses. The models are either individual-based models [9, 11, 12, 16, 23, 34, 39, 40, 46, 47] or continuum models [3, 13, 14, 26, 30, 31, 37, 44, 45].

The majority of the individual-based models investigate numerically the phase transitions between different behaviors [1, 11, 12, 47]. For example, Czirák et al. [11] derived a one-dimensional model that exhibits a transition from a disordered random behavior to a semizigzag behavior, which, for large time, evolves into a moving pulse. The authors also derived a continuum model which shows similar behavior [11]. However, for individual-based models there are no analytical techniques to understand such transitions. This lack of techniques causes difficulties in understanding the structure of these transitions, as well as which parameters determine these transitions: density [9], noise [11], or a combination of multiple parameters [18]. An illustrative example is the model by Vicsek et al. [47], which, without an analytical framework, was initially thought to exhibit a continuous transition from disordered to ordered motion (implying a supercritical bifurcation). Later, this transition has been shown to actually be discontinuous [18] (implying a subcritical bifurcation). Further results showed that the transition can be either continuous or discontinuous, depending on the way in which the noise is introduced [1]. However, the applicability of the results presented in [1] to the Vicsek model continues to be debated [7].

While the individual-based approach lacks a framework to analyze these transitions, for continuum models one can employ well-established analytical techniques to investigate them. In spite of these tools, there are not many articles investigating the various spatial and spatiotemporal patterns displayed by different continuum models that study animal aggregations. In particular, there are almost no results concerning the effects of the density and different model parameters on the structure of these group patterns. One exception is the model introduced in [45], which discusses the effect of the population size on the amplitude of stationary pulses.

This article attempts to address this lack of results. In particular, we will use analytical and numerical techniques to investigate some of the patterns exhibited by a nonlocal hyperbolic model for group formation that has been proposed in our previous work [13, 14]. The model introduces a general framework to incorporate different

communication mechanisms to study the formation of animal groups. In particular, these communication mechanisms influence the social interactions between individuals, namely attraction towards other members of the group that are far away, repulsion from those that are nearby, and a tendency to align with those neighbors that are at intermediate distances. The resulting model, which actually comprises many submodels, is very rich in spatial and spatiotemporal patterns. Numerical simulations have shown at least 10 different patterns, including stationary and traveling pulses, traveling trains, zigzag pulses, breathers, ripples, and a new pattern we called feathers. However, an analytical investigation of the patterns near bifurcation points is lacking. We begin to address this issue in the following.

For simplicity, we focus here *only on one* of the submodels introduced in [13]. The analysis in this article complements the work done in [14], which analyzes a similar submodel. More precisely, we will assume that for attractive and repulsive interactions, information received from all neighbors is used, whereas for alignment, only the information received from those neighbors moving towards an individual is used. It has been previously observed that this particular model displays at least four different spatial and spatiotemporal patterns: stationary pulses, traveling trains, semi-zigzag pulses, and traveling pulses [13]. Here, we will investigate the emergence of two of these patterns: stationary pulses and traveling trains. Both patterns occur near bifurcation points of the spatially homogeneous steady states.

Because of the nonlocal interactions, it is difficult to understand this model intuitively. One way to understand the obtained patterns is by a combination of numerical analysis, linear and weakly nonlinear analysis, and symmetry theory. Here we focus on numerical, linear, and weakly nonlinear analysis to investigate the stationary pulses and the traveling trains.

Note that a similar model was briefly analyzed in [14], where the authors investigated it via linear stability analysis. The linear stability analysis gives only information about the wavenumber that is most likely to emerge, and the parameter space where this will happen. However, the patterns observed during the numerical simulations are the result of the interactions between the nonlocal terms. Therefore, to better understand these patterns and, in particular, to reveal the complex structure of the possible attractors, we investigate the effect of these nonlinear terms. We use this analysis to answer the following biological questions: (1) How does the transition between disordered and ordered behaviors depend on the population density, or on social interactions? (2) Does this transition exhibit hysteresis, as observed in some individual-based models (see, e.g., [1,5])? (3) What is the effect of the alignment interactions on the structure of the animal groups?

We should mention that some of these questions can be somewhat answered by intensive numerical simulations. For example, it was observed in [14] that the transition between different types of ordered behavior can be explained in terms of the magnitude of the social interaction (e.g., attraction). However, the role of the population density on these transitions, as well as on the transition from disorder to ordered behavior, has not been investigated yet. Also, it should be mentioned that the results of the numerical simulations do not always offer a clear understanding of the mechanisms that govern such transitions, as shown by some individual-based models [1, 18, 47].

In the following, we will use the classical Landau–Stuart stability theory [28, 43] to analytically investigate the effects of the nonlocal interactions on the structure of two types of patterns: stationary pulses and traveling trains. We derive amplitude equations that govern the behavior of the solutions for large time, and investigate the stability of these solutions. The results show that both stationary pulses and traveling trains arise through subcritical bifurcations. We should mention here that the symmetries of the system can restrict the form of the solutions, as well as the amplitude equations (e.g., real versus complex amplitude equations) [17]. However, understanding the stability of the new bifurcating solutions depends on the values of the coefficients that appear in these equations, which necessitates detailed calculations. We then compare the analytical results for the amplitude of the solutions with the numerical results. Using the bifurcation diagrams for these amplitudes, we answer the biological questions we mentioned previously. In particular, we show that while increasing attraction leads to denser groups, increasing alignment has a dual effect, depending on whether the groups are stationary or moving. More precisely, increasing the alignment interaction makes the stationary groups more compact, and the moving groups more elongated. Moreover, we show the existence of a threshold for the total group density, above which coordinated behaviors, described by stationary and moving groups, are possible and persist for a very long time. In other words, groups that have the initial density below this threshold will disperse, while groups with densities above the threshold will become more dense, and persist for a long time. The analytical results also show that there is competition between the turning behavior and the magnitude of the alignment interaction that leads to the formation of stable aggregations. More precisely, in case of high-turning rates, increasing alignment decreases the amplitude of the perturbations required to destabilize the homogeneous solution. In case of low-turning rates, the situation is opposite: increasing alignment decreases the amplitude of the required perturbations.

The paper is organized as follows. In Sect. 2, we briefly describe the nonlocal hyperbolic model that we will analyze, and discuss the existence of solutions. In Sect. 3, we investigate the spatially homogeneous steady states and their stability via a linear stability analysis. In Sect. 4, we use weakly nonlinear analysis to study the amplitude of spatially and spatiotemporally heterogeneous solutions near bifurcation points. We conclude with a general discussion in Sect. 5. In the Appendix, we briefly introduce a two-dimensional analogue to the one-dimensional model introduced in [14].

2 Hyperbolic model and the existence of solutions

In [13, 14] the authors introduced the following one-dimensional hyperbolic model to describe the evolution of densities of right-moving (u^+) and left-moving (u^-) individuals:

$$\begin{aligned}\partial_t u^+(x, t) + \partial_x(\gamma u^+(x, t)) &= -\lambda^+(u^+, u^-)u^+(x, t) + \lambda^-(u^+, u^-)u^-(x, t), \\ \partial_t u^-(x, t) - \partial_x(\gamma u^-(x, t)) &= \lambda^+(u^+, u^-)u^+(x, t) - \lambda^-(u^+, u^-)u^-(x, t), \quad (1) \\ u^\pm(x, 0) &= u_0^\pm(x), \quad x \in \mathbf{R},\end{aligned}$$

with the turning rates defined as

$$\lambda^\pm(u^+, u^-) = \lambda_1 + \lambda_2 h(y^\pm[u^+, u^-]). \quad (2)$$

Here γ is the constant speed, while the two constants λ_1 and λ_2 represent a “base-line” turning rate and a bias turning rate, respectively. For a biologically realistic case, the turning function h should be a positive, increasing, and bounded functional that depends on the signals perceived from neighbors: y^\pm . These signals are emitted by neighbors moving to the right (u^+) and to the left (u^-):

$$\begin{aligned} y^\pm[u^+, u^-] = & \pm q_r \int_0^\infty K_r(s) (u(x \pm s, t) - u(x \mp s, t)) ds \\ & \mp q_a \int_0^\infty K_a(s) (u(x \pm s, t) - u(x \mp s, t)) ds \\ & \pm q_{al} \int_0^\infty K_{al}(s) (u^\mp(x \pm s, t) - u^\pm(x \mp s, t)) ds. \end{aligned} \quad (3)$$

We define the total density as $u(x, t) = u^+(x, t) + u^-(x, t)$. The constants q_r , q_a , and q_{al} represent the magnitudes of three social interactions: repulsion, attraction, and alignment, respectively. In (3), we assume that, for attractive and repulsive interactions, information received from all neighbors ($u(x + s, t)$ and $u(x - s, t)$) is used. For alignment interactions, on the other hand, only the information received from those neighbors moving towards a particular individual ($u^-(x + s, t)$ and $u^+(x - s, t)$) is used. A more detailed description of these equations can be found in [14].

Throughout this paper, the interaction kernels K_j , $j = r, al, a$, are described by:

$$K_j(s) = \frac{1}{\sqrt{2\pi m_j^2}} \exp\left(-\frac{(s - s_j)^2}{2m_j^2}\right), \quad j = r, al, a. \quad (4)$$

Here s_j , $j = r, al, a$, define the spatial regions for repulsive, alignment, and attractive interactions, while $m_j = s_j/8$ define the width of these regions. We choose the constants m_j such that the support of more than 98% of the mass of the kernels is inside the interval $[0, \infty)$. Note that in [14], the kernels had overlapping ranges. The translated Gaussian kernels (4) we use in this article have quite distinct ranges, which allows for better comparison with individual-based models. In Sects. 3 and 4, we investigate a specific case where the positive, bounded, and increasing turning functions are defined by

$$h(y^\pm[u^+, u^-]) = 0.5 + 0.5 \tanh(y^\pm[u^+, u^-] - y_0). \quad (5)$$

Note that there are many other possible choices for the turning functions (e.g., piecewise linear functions). However, it is beyond the scope of this paper to investigate

them. The constant y_0 is chosen such that for $y^\pm[v] = 0$ (that is, no signals), the value of $\lambda^\pm(0)$ is determined only by λ_1 .

It should be mentioned that the full system (1)–(4) has 14 parameters. Since the nondimensionalization does not significantly reduce the number of parameters (we still have ten parameters), we simply work with the dimensional system.

A first result refers to the existence of weak solutions of system (1). In the mathematical literature, there are results for the existence and uniqueness of solutions for hyperbolic systems of the form (1), with local turning rates defined as $\lambda^+(u^+, u^-) = \lambda^-(u^-, u^+)$ (see [25]), or $\lambda^\pm = \lambda^\pm(s, s_x)$, where s is an external stimulus that depends on u^\pm (see [22]). In contrast to these cases, the model discussed here has nonlocal turning rates.

If we assume that the initial data is $u_0^\pm \in L^\infty(\mathbf{R})$, the turning rates are locally Lipschitz continuous as functions of the signals y^\pm , and the kernels $K_j \in L^1(\mathbf{R})$, $j = a, r, al$, then we can prove that there exists a unique mild solution $u^\pm \in L^\infty(\mathbf{R} \times [0, \infty))$. A sketch of the proof is presented in Appendix 2. Note that if the initial data $u_0^\pm(x)$ is periodic, then the solution u^\pm is periodic (see also the proofs in [21, 25]). Therefore, this theorem is valid on a bounded domain with periodic boundary conditions.

3 Spatially homogeneous steady states and linear analysis

It has been previously shown [13] that system (1) with kernels defined by (4) exhibits at least four types of spatial patterns: stationary pulses, traveling trains, traveling pulses, and semi-zigzag pulses. To understand the origin of these patterns, we will first study the behavior of small perturbations of the spatially homogeneous steady states, that is, the states that have both right-moving and left-moving individuals evenly spread over the domain. The growth of these perturbations gives us the first conditions on the parameters that determine when these steady states become linearly unstable and form spatial and spatiotemporal patterns (i.e., spatially heterogeneous solutions).

Note that a similar analysis of the number and stability of the steady state solutions of system (1) has been carried out in [14]. In the following, we will briefly summarize these results since they are particularly important for the weakly nonlinear analysis shown in Sect. 4.

As mentioned in Introduction, the turning function we use is described by (5). Moreover, we assume that system (1)–(4) is defined on a bounded domain $[0, L]$ with wrap-around boundary conditions for the nonlocal interaction terms (see [14] for further discussion). This leads to a discrete set of unstable modes that will give rise to spatial and spatiotemporal patterns. Let us define the total population density to be $A = \frac{1}{L} \int_0^L (u^+ + u^-)(x, t) dx$. The spatially homogeneous steady states of (1) are the solutions $(u^+, u^-) = (u^*, A - u^*)$ of the steady-state equation

$$0 = H(u^*; q_{al}, \lambda, A) := -u^* (\lambda_1 + \lambda_2 0.5 + \lambda_2 0.5 \tanh(Aq_{al} - 2u^*q_{al} - y_0)) + (A - u^*) (\lambda_1 + \lambda_2 0.5 + \lambda_2 0.5 \tanh(-Aq_{al} + 2u^*q_{al} - y_0)). \tag{6}$$

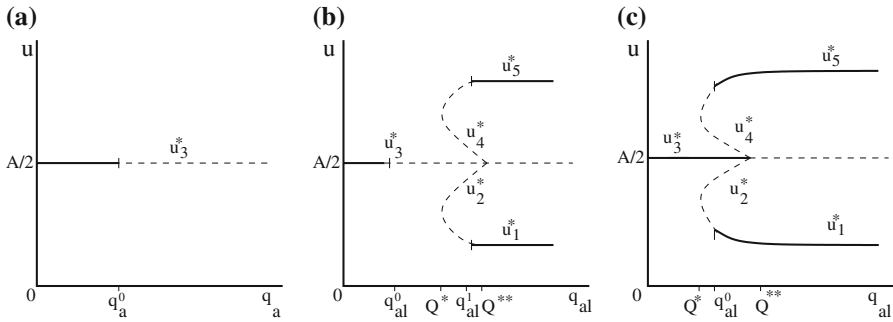


Fig. 1 Bifurcation diagrams for the steady-state equation. **a** Zero alignment ($q_{al} = 0$); the only steady state is $u_3^* = A/2$. **b** Nonzero alignment ($q_{al} \neq 0$); $(u_3^*, u_3^*) = (A/2, A/2)$ is always a steady state; at the critical value $q_{al} = Q^*$, four new steady states appear through a saddle-node bifurcation. These states can be any of the following pairs: (u_1^*, u_5^*) , (u_5^*, u_1^*) , (u_2^*, u_4^*) , (u_4^*, u_2^*) . At a second critical value of the alignment parameter, $q_{al} = Q^{**}$, two of these spatially homogeneous steady states (u_2^* and u_4^*) disappear through a subcritical pitchfork bifurcation. **c** A particular case of **b**, obtained for a different parameter space. In all three cases, the solid lines denote the stable solution, while the dashed lines denote the unstable solution (with respect to spatial perturbations). Shown here is the stability of the steady states to small spatial perturbations when: **a** $q_{al} = 0$, $q_r = 2.2$, $\lambda_1 = 0.2$, $\lambda_2 = 0.9$, $\gamma = 0.1$, $A = 2$; here q_a is the bifurcation parameter; at $q_a = q_a^0$ there is a real bifurcation; **b** $q_a = q_r = 0$, $\lambda_1 = 0.2/0.7$, $\lambda_2 = 0.9/0.7$, $\gamma = 0.1$, $A = 2$; (u_3^*, u_3^*) undergoes a real bifurcation at $q_{al} = q_{al}^0$, while (u_1^*, u_5^*) undergoes an imaginary bifurcation at $q_{al} = q_{al}^1$; **c** $q_a = q_r = 0$, $\lambda_1 = 2.0$, $\lambda_2 = 9.0$; at $q_{al} = q_{al}^0$ there is an imaginary bifurcation

Note that (6) is similar to the one obtained in [14], where the attractive and repulsive interactions were described by odd kernels. The reason for this is that the interactions are defined in terms of the total density $u = u^+ + u^-$ [see (3)], and therefore, (6) depends only on the alignment coefficient q_{al} , and not on q_a and q_r .

When attraction and repulsion are the only possible social interactions (i.e., $q_{al} = 0$), the only spatially homogeneous steady state is $(u^+, u^-) = (A/2, A/2)$ (Fig. 1a). However, when alignment plays a role in the social interactions (i.e., $q_{al} \neq 0$), (6) can have one, three, or five solutions, as shown in Fig. 1b and c. We will denote these five solutions by u_i^* , $i = 1 \dots 5$. Therefore, the spatially homogeneous steady states generically denoted by $(u^*, u^{**}) = (u^*, A - u^*)$ can be any of the following pairs: (u_1^*, u_5^*) , (u_5^*, u_1^*) , (u_2^*, u_4^*) , (u_4^*, u_2^*) , or $(u_3^*, u_3^*) = (A/2, A/2)$.

The stability of these solutions depends on the parameter space. To investigate this stability, we consider small perturbations caused by spatially nonhomogeneous terms: $u^+(x, t) = u^* + u_p(x, t)$ and $u^-(x, t) = u^{**} + u_m(x, t)$. Let $u_{p,m}(x, t) \propto e^{\sigma t + ikx}$, with the wave number k and the growth rate σ . Note that the wrap-around boundary conditions require that the wave number k attains only discrete values $k_n = 2n\pi/L$, $n \in \mathbf{N}$. Because of the conservation of the total density, $k_0 = 0$ is not an allowable wave number and hence, $n \in \mathbf{N}^+$. If we substitute the expressions for $u^\pm(x, t)$ into system (1), we obtain the dispersion relation

$$\sigma^2 + \sigma C(k) + D(k) = 0, \tag{7}$$

where

$$\begin{aligned}
 C(k) &= L_1 + L_2 - M_5 q_{al} (\hat{K}_{al}^+(k) + \hat{K}_{al}^-(k)), \\
 D(k) &= \gamma^2 k^2 + \gamma ik \left(L_2 - L_1 + M_5 q_{al} (\hat{K}_{al}^-(k) - \hat{K}_{al}^+(k)) \right) \\
 &\quad - 2M_5 \gamma ik \left(q_r (\hat{K}_r^+ - \hat{K}_r^-) - q_a (\hat{K}_a^+ - \hat{K}_a^-) \right), \\
 L_1 &= \lambda_1 + \lambda_2 0.5 + \lambda_2 0.5 \tanh(M_1 - y_0), \\
 L_2 &= \lambda_1 + \lambda_2 0.5 + \lambda_2 0.5 \tanh(-M_1 - y_0), \\
 P_1 &= \lambda_2 0.5 (1 + \tanh^2(M_1 - y_0)), \\
 P_2 &= \lambda_2 0.5 (1 + \tanh^2(-M_1 - y_0)), \\
 M_1 &= q_{al} (u^{**} - u^*), \\
 M_5 &= P_1 u^* + P_2 u^{**}.
 \end{aligned}
 \tag{8}$$

Here, $\hat{K}_j, j \in \{a, r, al\}$, are the Fourier transforms of the interaction kernels (4):

$$\hat{K}_j^\pm(k) = \int_{-\infty}^{\infty} K_j(s) e^{\pm iks_j} ds = \exp(\pm is_j k - k^2 m_j^2 / 2).
 \tag{9}$$

Note that these integrals are defined on the entire real line, whereas (3) are defined on $[0, \infty)$. Since the constants $m_j, j = r, al, a$ were chosen such that the support of more than 98% of the mass of the kernels is inside the interval $[0, \infty)$, we can approximate the integrals defined on $[0, \infty)$ by integrals on $(-\infty, \infty)$ (see also [14]).

Equations (7)–(8) say that the steady state $(u^+, u^-) = (u^*, u^{**})$ is unstable, that is $\Re(\sigma(k)) > 0$, when $C(k) < 0$ or $D(k) < 0$. The first term, $C(k)$, is negative when λ_2 is large. Similar to the case discussed in [14], the term $D(k)$ is negative when (a) λ_2 is large, or when (b) attraction is larger than repulsion : $q_a \left(\hat{K}_a^+(k) - \hat{K}_a^-(k) \right) > q_r \left(\hat{K}_r^+(k) - \hat{K}_r^-(k) \right)$. When λ_2 is large, the unstable modes are those with large k . When attraction is larger than repulsion, the modes with small k are unstable. We will come back to this result in Sect. 4, when we will investigate the contribution of the nonlinear terms to the final pattern.

Figure 1 shows three types of bifurcation diagrams obtained for system (1). Since these bifurcations are the starting point for the weakly nonlinear analysis discussed in Sect. 4, we will discuss them in detail. In Fig. 1a, there is a critical value of attraction $q_a = q_a^0$ such that the steady state u_3^* is stable for $q_a < q_a^0$, and unstable otherwise. In Fig. 1b and c, the bifurcation parameter is q_{al} . Figure 1b shows that, in some parameter space, there exists a critical value $q_{al}^0 < Q^*$ such that for $q_{al} < q_{al}^0$, the solution u_3^* is stable, while for $q_{al} > q_{al}^0$ it is unstable. The relative position of the bifurcation point depends on the parameter space. Such an example is shown in Fig. 1c where

the bifurcation point at which u_3^* changes stability coincides with Q^{**} . Actually, for $q_{al} > Q^{**}$, u_3^* is always unstable, independent of the parameter space. Also, there exists a critical value of alignment q_{al}^0 such that the steady states u_1^* and u_5^* are unstable for $q_{al} < q_{al}^0$ and stable otherwise, as seen in Fig. 1c. In Fig. 1b, this critical value of alignment is denoted q_{al}^1 . The other two steady states, u_2^* and u_4^* , are always unstable. Moreover, numerical simulations suggest that the solutions perturbed from u_2^* and u_4^* go to the same attractor as the solutions perturbed from the other three steady states (u_1^* , u_3^* , and u_5^*). For this reason, we will ignore u_2^* and u_4^* for the rest of the paper.

It should be noted that, when $u^* \neq u^{**}$, equation (7) is complex. However, for $u^* = u^{**}$, it is real. This has implications on the type of the eigenvalues of system (1). For the first case, all eigenvalues are complex. For the second case, the eigenvalues can be real or complex, depending on the values of the parameters.

The spatially homogeneous solutions that become unstable when $\Re(\sigma(k)) > 0$ are eventually bounded by nonlinear terms. In the following section, we will take into consideration these nonlinear terms and use them to derive amplitude equations that govern the behavior of the solutions for large time.

4 Nonlinear analysis

The previous linear stability analysis is only valid for small time and infinitesimal perturbations. For large time, the nonlinear terms dominate the growth of the unstable modes. To study the influence of these nonlinear terms on the final heterogeneous pattern, we will employ the classical method of weakly nonlinear analysis (see [28, 43]). The method uses separate time scales to study how the amplitude of the heterogeneous solution varies with time. More precisely, there is a fast time scale and a slow time scale. The fast time scale is represented by the initial time region (t) where the solution starts to develop. This is the time scale where the linear stability analysis is valid. The slow time scale is represented by a second time region ($T = \epsilon^2 t$) where the effects of the nonlinear terms become important. Here, the amplitude of these heterogeneous patterns varies slowly. The two time variables t and T are considered to be independent as ϵ approaches zero.

In this section, we study the patterns that bifurcate from the spatially homogeneous steady state (u^* , u^{**}). Figure 2 shows two patterns that emerge through a real bifurcation [cases (a) and (b)], and two patterns that emerge through an imaginary bifurcation [cases (c) and (d)]. Figure 2a describes a single stationary pulse obtained for large attractive interactions (q_a). Figure 2b describes multiple stationary pulses which are obtained for large turning rates (λ_2). Figure 2c describes a traveling train formed of one peak, obtained for large attraction. Figure 2d describes a traveling train formed of 17 peaks, and obtained for large turning rates. We should note here that we define a traveling train to be a pattern that doubles the number of its peaks as we double the domain size. A traveling pulse, on the other hand, has the same number of peaks as we double the domain size. By this definition, the pattern shown in Fig. 2c is a traveling train, since doubling the domain size leads to the formation of two moving groups. It has been observed numerically [13] that the hyperbolic system (1) exhibits two more

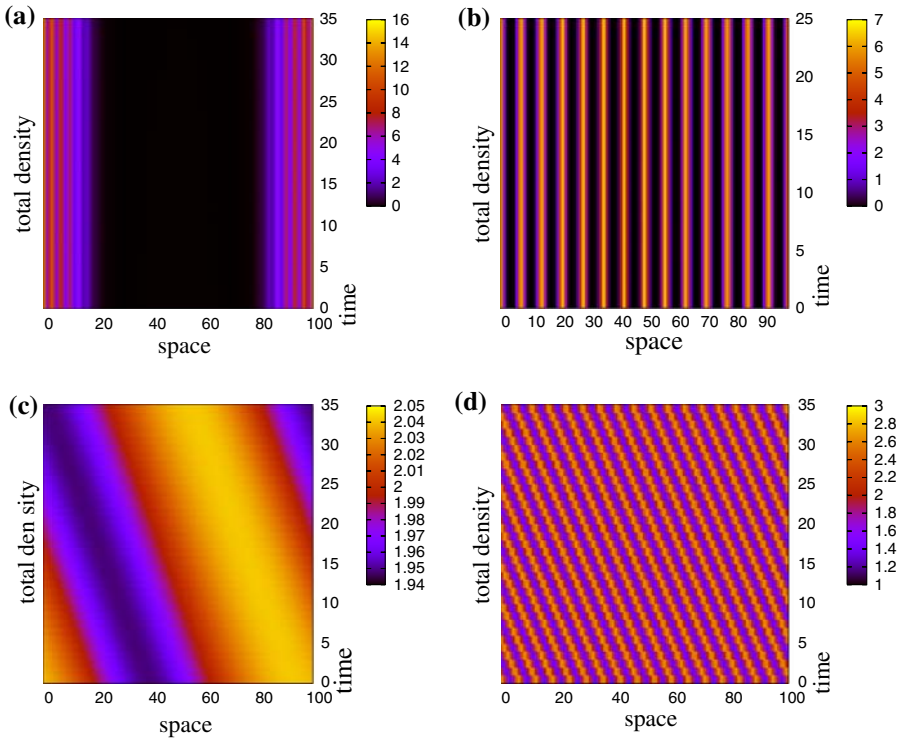


Fig. 2 Patterns exhibited by system (1). Shown is the total density $u(x, t) = u^+(x, t) + u^-(x, t)$. **a** Stationary pulses; $q_a = 0.93, q_r = 2.2, q_{al} = 0, \lambda_1 = 0.2, \lambda_2 = 0.9, \gamma = 0.1$. **b** Stationary pulses; $q_r = q_a = 0, q_{al} = 0.85, \lambda_1 = 2.0, \lambda_2 = 9.0, \gamma = 0.1$. **c** Traveling train; $q_a = 1.0, q_r = 0.1, q_{al} = 2.45, \lambda_1 = 0.2, \lambda_2 = 0.9$. **d** Traveling trains; $q_a = q_r = 0, q_{al} = 2.08, \lambda_1 = 0.2/0.7, \lambda_2 = 0.9/0.7, \gamma = 0.1$

patterns, namely traveling pulses and semi-zigzag pulses. Since both patterns occur far from the bifurcation point, we will not discuss them in this paper.

In Sects. 4.1 and 4.2, we focus on the situation when the bifurcation occurs at a real eigenvalue. As previously mentioned, the spatially homogeneous steady state is $(u^*, u^{**}) = (u_3^*, u_3^*)$. We first analyze system (1) when only attractive and repulsive interactions are present (that is, $q_r, q_a \neq 0, q_{al} = 0$). In this case, previous results [14] have shown that it is possible to obtain stationary heterogeneous patterns, such as the single stationary pulse shown in Fig. 2a. At the end of Sect. 4.2, we will briefly discuss the case when $q_a = q_r = 0$ and $q_{al} \neq 0$. In this case it is possible to obtain multiple stationary pulses, such as those shown in Fig. 2b. In Sects. 4.3 and 4.4, we will study a bifurcation that occurs at a purely imaginary eigenvalue. The focus will be on the steady state $(u^*, u^{**}) = (u_1^*, u_5^*)$. To keep the results tractable, we will consider the situation when alignment is the only social interaction (that is, $q_{al} \neq 0, q_a = q_r = 0$). In this case, we obtain spatiotemporal patterns described by traveling trains, as shown in Fig. 2d. At the end of Sect. 4.4, we will briefly discuss the situation when we include repulsive and attractive interactions. The traveling train pattern that results in this case is shown in Fig. 2c.

4.1 Weakly nonlinear analysis in the neighborhood of a real bifurcation

In this section, we will consider only attractive and repulsive social interactions (that is, $q_a = 0$). As mentioned, the only spatially homogeneous steady state is $(u^*, u^{**}) = (A/2, A/2)$. We are interested in the stability of this steady state as we increase the magnitude of attraction (q_a). Let us denote by q_a^0 the critical value of q_a for which the dispersion relation satisfies $\sigma(q_a^0, k_c) = 0$ (the case is depicted in Fig. 1a). Let $k = k_c$ be the critical wave number. A solution of (1) near the bifurcation point is given by

$$u^\pm(x, t) \propto e^{\sigma t + ik_c x} + \text{c.c.}, \quad (10)$$

where “c.c.” stands for “complex conjugate”. We perform a perturbation analysis in a neighborhood of the critical value (q_a^0):

$$q_a = q_a^0 + v\epsilon^2, \quad 0 < \epsilon \ll 1, \quad v = \pm 1. \quad (11)$$

Writing the dispersion relation in a power series about q_a^0 , namely

$$\sigma(q_a, k_c) = \sigma(q_a^0, k_c) + \frac{\partial \sigma(q_a^0, k_c)}{\partial q_a} \epsilon^2 v + O(\epsilon^4), \quad (12)$$

and substituting it into (10) gives us

$$e^{\sigma(q_a, k_c)t + ik_c x} = e^{ik_c x + \frac{d\sigma(q_a^0, k_c)}{dq_a} v \epsilon^2 t} \approx e^{ik_c x} \alpha(\epsilon^2 t). \quad (13)$$

The amplitude α depends on the slow time $\epsilon^2 t$. This suggests we introduce a new time variable $T = \epsilon^2 t$ and consider fast and slow time scales, t^* and T , respectively:

$$t \rightarrow t^* + T. \quad (14)$$

In the limit $\epsilon \rightarrow 0$ we treat these two time scales as being independent [32]. We denote $\tilde{u}^\pm(x, t^*, \epsilon, T) = u^\pm(x, t)$. For notational simplicity, we drop the asterisk and the tilde, and assume the following formal expansion

$$\begin{aligned} u^+(x, t, \epsilon, T) &= u^* + \epsilon u_1^+ + \epsilon^2 u_2^+ + \epsilon^3 u_3^+ + O(\epsilon^4), \\ u^-(x, t, \epsilon, T) &= u^{**} + \epsilon u_1^- + \epsilon^2 u_2^- + \epsilon^3 u_3^- + O(\epsilon^4). \end{aligned} \quad (15)$$

We then expand the nonlinear function $\tanh(y^\pm[u^+, u^-] - y_0) = \tanh(y^\pm[u^*, u^{**}] + \sum_j \epsilon^j y^\pm[u_j^+, u_j^-] - y_0)$ in a Taylor series about $y^\pm[u^*, u^{**}]$. The turning functions

(2) and (5) can therefore be written as

$$\begin{aligned} \lambda^\pm = & L_{1,2} + P_{1,2} \sum_j \epsilon^j y^\pm [u_j^+, u_j^-] + S_{1,2} \left(\sum_j \epsilon^j y^\pm [u_j^+, u_j^-] \right)^2 \\ & + T_{1,2} \left(\epsilon^j \sum_j y^\pm [u_j^+, u_j^-] \right)^3 + O(\epsilon^4), \quad j = 1, 2, 3, \dots, \end{aligned} \tag{16}$$

with $L_{1,2}$ and $P_{1,2}$ defined by (8), and

$$\begin{aligned} S_1 &= \frac{\lambda_2}{2} \tanh(M_1 - y_0) \left(1 - \tanh^2(M_1 - y_0) \right), \\ S_2 &= \frac{\lambda_2}{2} \tanh(-M_1 - y_0) \left(1 - \tanh^2(-M_1 - y_0) \right), \\ T_1 &= \frac{\lambda_2}{12} \left(-(1 - \tanh(M_1 - y_0))^2 + 4 \tanh(M_1 - y_0)^2 (1 - \tanh(M_1 - y_0)^2) \right), \\ T_2 &= \frac{\lambda_2}{12} \left(-(1 - \tanh(-M_1 - y_0))^2 + 4 \tanh(-M_1 - y_0)^2 (1 - \tanh(-M_1 - y_0)^2) \right). \end{aligned}$$

Since we consider $q_{al} = 0$, this implies that $M_1 = 0, L_1 = L_2, P_1 = P_2, S_1 = S_2$, and $T_1 = T_2$.

The nonlinear system (1) can be written as

$$\mathbf{N}(\mathbf{u}) = 0, \tag{17}$$

with $\mathbf{u} = (u^+, u^-)^T$. Substituting expressions (15) and (16) into this equation leads to $\mathbf{N}(\sum_{j=1} \epsilon^j \mathbf{u}_j) = \sum_j \mathbf{N}_j(\mathbf{u}_j) \epsilon^j$. At each $O(\epsilon^j)$, we can write $\mathbf{N}_j(\mathbf{u}_j) = L(\mathbf{u}_j) - N_j - E_j$. Here $L(\mathbf{u}_j)$ represents the linear part of the system (1), N_j contains the nonlinear terms formed of u_{j-1}^\pm, u_{j-2}^\pm , etc., and E_j contains the slow time derivatives $\partial_T u_{j-2}^\pm$, ($j \geq 3$) and the terms multiplied by v . The linear operator L is the same at each $O(\epsilon^j)$ step, whereas N_j and E_j have to be calculated every time. Therefore, $\mathbf{N}_j(\mathbf{u}_j) = 0$ reduces to

$$L(\mathbf{u}_j) = N_j + E_j, \quad j = 1, 2, 3, \dots \tag{18}$$

Since the eigenvalues are real, the spatially homogeneous steady state becomes linearly unstable to spatial patterns, and therefore, the linear operator L is defined as

$$L(\mathbf{u}) = \begin{pmatrix} \gamma \partial_x + L_1 + M_5 K * \cdot & -L_1 + M_5 K * \cdot \\ -L_1 - M_5 K * \cdot & -\gamma \partial_x + L_1 - M_5 K * \cdot \end{pmatrix} \begin{pmatrix} u^+ \\ u^- \end{pmatrix}, \tag{19}$$

where the convolution $K * \cdot$ is defined by

$$K * u^\pm = q_r \left(\tilde{K}_r * u^\pm - K_r * u^\pm \right) - q_a^0 \left(\tilde{K}_a * u^\pm - K_a * u^\pm \right), \tag{20}$$

with $\tilde{K}_{r,a}(s) = K_{r,a}(-s)$, and $(K_{r,a} * u^\pm)(x) = \int_{-\infty}^{\infty} K_{r,a}(s)u^\pm(x-s)ds$. Throughout the analysis, we will use the operator L_{k_c} , which is obtained by applying L to solutions of the form $e^{ik_c x}$:

$$L_{k_c} = \begin{pmatrix} \gamma i k_c + L_1 + M_5 \hat{K}^+(k_c) & -L_1 + M_5 \hat{K}^+(k_c) \\ -L_1 - M_5 \hat{K}^+(k_c) & -\gamma i k_c + L_1 - M_5 \hat{K}^+(k_c) \end{pmatrix}. \quad (21)$$

Here we define $\hat{K}^+(k_c) = q_r \left(\hat{K}_r^+(k_c) - \hat{K}_r^-(k_c) \right) - q_a^0 \left(\hat{K}_a^+(k_c) - \hat{K}_a^-(k_c) \right)$, where \hat{K}_j^\pm , $j = r, a$ are the Fourier transforms (9). Later, we will also use $\hat{K}^-(k_c) = -\hat{K}^+(k_c)$, $\hat{K}^+(2k_c)$, and $\hat{K}^-(2k_c) = -\hat{K}^+(2k_c)$. At $O(\epsilon^1)$, the nonlinear terms are $N_1 = E_1 = 0$, and therefore (17) reduces to solving

$$L(\mathbf{u}) = \mathbf{0}. \quad (22)$$

This linear equation has a nontrivial solution. Therefore, for $O(\epsilon^j)$, $j \geq 2$, the nonlinear equation (18) has a solution if and only if $N_j + E_j$ satisfies the Fredholm alternative [24]. However, to be able to apply the Fredholm alternative, one has to investigate whether the linear operator L is compact.

Throughout this section, we consider the Hilbert space

$$Y = \left\{ \mathbf{v}(x, \tau) \mid (x, \tau) \in [0, L] \times [0, \infty), \text{ s.t. } \lim_{T \rightarrow \infty} \frac{1}{T} \int_0^T \int_0^L |\mathbf{v}|^2 dx d\tau < \infty \right\}, \quad (23)$$

with the inner product

$$\langle \mathbf{v}, \mathbf{w} \rangle = \lim_{T \rightarrow \infty} \frac{1}{T} \int_0^T \int_0^{L=\frac{2\pi}{k_c}} (v^1 \bar{w}^1 + v^2 \bar{w}^2) dx d\tau, \quad (24)$$

where $\mathbf{v} = (v^1, v^2)^T$, $\mathbf{w} = (w^1, w^2)^T$. Moreover, we will assume that u^\pm satisfy periodic boundary conditions.

Note that since u^\pm are bounded on $L^\infty([0, L] \times [0, T])$ (see Appendix 2), they are also bounded on $L^2([0, L] \times [0, T])$ [41]. Therefore, the limit $\lim_{T \rightarrow \infty} \frac{1}{T} \|\mathbf{v}\|_{L^2([0, L] \times [0, T])}^2$ is finite.

Let us now rewrite the linear operator $L = \gamma L_d + L_0$, where L_d is the differential operator

$$L_d(\mathbf{u}) = \begin{pmatrix} \partial_x & 0 \\ 0 & -\partial_x \end{pmatrix} \begin{pmatrix} u^+ \\ u^- \end{pmatrix}, \quad (25)$$

and L_0 is described by

$$L_0(\mathbf{u}) = \begin{pmatrix} L_1 + M_5 K * \cdot & -L_1 + M_5 K * \cdot \\ -L_1 - M_5 K * \cdot & L_1 - M_5 K * \cdot \end{pmatrix} \begin{pmatrix} u^+ \\ u^- \end{pmatrix}. \tag{26}$$

Note that the operator L_0 is compact (since the integral operator K is compact (see, e.g., [41], Section 3.4)). The problem is caused by the differential operator L_d which is not bounded [41]. This issue can be addressed following the approach shown in [27], where the differential operator is interpreted as a distribution in a Sobolev subspace of Y , which requires the derivatives to be also in Y . This way, the distributional interpretation defines the operator on a closed domain in Y . In a similar manner, we can restrict the definition of the linear operator L to act on the Sobolev subspace. The adjoint of this linear operator, L^* , acts on elements of Y in the following manner:

$$L^*(\mathbf{u}) = \begin{pmatrix} -\gamma \partial_x + L_1 + M_5 \hat{K}^* * \cdot & -L_1 - M_5 \hat{K}^* * \cdot \\ -L_1 + M_5 \hat{K}^* * \cdot & \gamma \partial_x + L_1 - M_5 \hat{K}^* * \cdot \end{pmatrix} \begin{pmatrix} u^+ \\ u^- \end{pmatrix}, \tag{27}$$

where K^* describes the adjoint integral operator.

Following similar steps as in [27], it can be shown that the kernel of the above restricted operator is finite-dimensional, and its range is closed. Therefore, the Fredholm alternative can be applied, which means that $N_j + E_j$ has to be orthogonal to the bounded solution of the adjoint homogeneous problem

$$L^*(\hat{\mathbf{u}}) = 0. \tag{28}$$

Let us consider this solution $\hat{\mathbf{u}} = (\hat{u}^+, \hat{u}^-)^T$ to be defined by

$$\hat{\mathbf{u}} = \beta_1(T) \mathbf{W} e^{ik_c x} + \beta_2(T) \bar{\mathbf{W}} e^{-ik_c x}. \tag{29}$$

Then (28) results in

$$\bar{L}_{k_c}^T(\hat{\mathbf{u}}) = 0, \tag{30}$$

with the adjoint operator defined as

$$\bar{L}_{k_c}^T = \begin{pmatrix} -\gamma i k_c + L_1 + M_5 \hat{K}^-(k_c) & -L_1 - M_5 \hat{K}^-(k_c) \\ -L_1 + M_5 \hat{K}^-(k_c) & \gamma i k_c + L_1 - M_5 \hat{K}^-(k_c) \end{pmatrix}. \tag{31}$$

The orthogonality condition reads

$$\langle \hat{\mathbf{u}}, \overline{(\mathbf{N}_j + \mathbf{E}_j)} \rangle = 0. \tag{32}$$

We are interested only in those terms of $\mathbf{N}_i + \mathbf{E}_i$ that contain $e^{\pm i k_c x}$ since these terms give rise to secular solutions. For the particular case we study here, the secular terms

appear at $O(\epsilon^3)$. The nonlinear interactions $\mathbf{N}_3 + \mathbf{E}_3$ are described by

$$\begin{aligned} \mathbf{N}_3 + \mathbf{E}_3 = & \frac{\partial \alpha}{\partial T} e^{ik_c x} \mathbf{R}^{(3)} + \frac{\partial \bar{\alpha}}{\partial T} e^{-ik_c x} \bar{\mathbf{R}}^{(3)} + \alpha e^{ik_c x} \nu \mathbf{R}^{(2)} + \bar{\alpha} e^{-ik_c x} \nu \bar{\mathbf{R}}^{(2)} \\ & + \alpha |\alpha|^2 e^{ik_c x} \mathbf{R}^{(1)} + \bar{\alpha} |\alpha|^2 e^{-ik_c x} \bar{\mathbf{R}}^{(1)} + \text{other terms}, \end{aligned} \quad (33)$$

where ‘‘other terms’’ describe those terms of the form $e^{\pm 2ik_c x}$, $e^{\pm 3ik_c x}$, etc. The coefficients $\mathbf{R}^{(1)}$, $\mathbf{R}^{(2)}$, and $\mathbf{R}^{(3)}$ are given in Appendix 3. Substituting this expression into the orthogonality condition leads to the following amplitude equation:

$$\frac{d\alpha}{dT} = -\nu \alpha Y - \alpha |\alpha|^2 X, \quad (34)$$

where

$$Y = \frac{\bar{\mathbf{W}} \cdot \mathbf{R}^{(2)}}{\bar{\mathbf{W}} \cdot \mathbf{R}^{(3)}}, \quad X = \frac{\bar{\mathbf{W}} \cdot \mathbf{R}^{(1)}}{\bar{\mathbf{W}} \cdot \mathbf{R}^{(3)}}. \quad (35)$$

We can verify that

$$Y = \frac{d\sigma}{dq_a} = \frac{\gamma ik M_5 (\hat{K}_a^+ - \hat{K}_a^-)}{L_1}. \quad (36)$$

Therefore the linear approximation of this amplitude equation agrees with the linear prediction given by the dispersion relation (12).

The amplitude equation (34) is complex. To obtain a real equation, let us define $\alpha(T) = R(T)e^{i\theta(T)}$, with real terms $R(T) = |\alpha|$ and $\theta(T)$. Thus, equation (34) can be rewritten as

$$\frac{dR}{dT} = -\nu R \Re(Y) - R^3 \Re(X), \quad (37)$$

$$\frac{d\theta}{dT} = -\nu \Im(Y) - R^2 \Im(X), \quad (38)$$

with \Re and \Im denoting the real and imaginary parts of the two coefficients X and Y . The two steady-state solutions of (37) are $R = 0$ and $R = \sqrt{-\nu \Re(Y) / \Re(X)}$. To study the stability of these solutions, we write $R = R_0 + R_\delta$, where R_0 is the steady state and R_δ is a small perturbation. Equation (37) then becomes

$$\frac{dR_\delta}{dT} = R_\delta \left(-\nu \Re(Y) - 2R_0^2 \Re(X) \right). \quad (39)$$

We can observe that the trivial state $R_0 = 0$ is stable if $\nu \Re(Y) > 0$, and unstable otherwise. The nontrivial state $R_0 = \sqrt{-\nu \Re(Y) / \Re(X)}$ is unstable if $\nu \Re(Y) > 0$, and stable otherwise.

Figure 3 shows the variation of the amplitude for the stationary pulses described in Fig. 2a. For $u_3^* = A/2 = 1$, $q_r = 2.2$, $q_{al} = 0$, $\gamma = 0.1$, $\lambda_1 = 0.2$, $\lambda_2 = 0.9$,

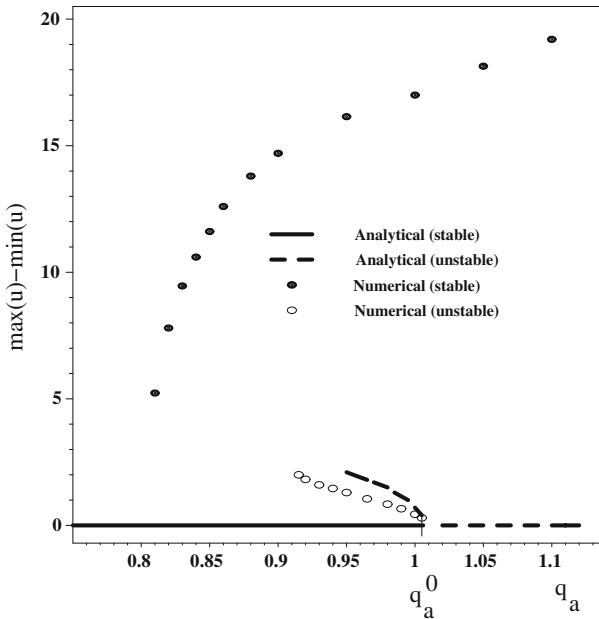


Fig. 3 The amplitude of the spatially heterogeneous solution $u(x, t) = u^+(x, t) + u^-(x, t)$ as we perturb the magnitude of attraction q_a . The *dashed curves* represent the unstable branch obtained using the weakly nonlinear analysis. The *solid circles* represent the stable branch obtained numerically, whereas the *open circles* represent the unstable branch obtained numerically. The critical value of q_a is $q_a^0 = 1.008$. The other parameters are: $\lambda_1 = 0.2$, $\lambda_2 = 0.9$, $\gamma = 0.1$, $q_r = 2.2$, $q_{al} = 0$, $y_0 = 2$. For $q_a < q_a^0$, the zero amplitude branch (corresponding to $|\alpha^2| = 0$) is stable (*continuous line*). For $q_a > q_a^0$ it becomes unstable (*dashed line*). When $q_a < q_a^0$, the curve formed by the open circles marks the boundary of the stability region, as determined numerically. Perturbations with amplitude on or above this curve grow to the upper branch (*solid circles*), while perturbations with amplitude below this curve decay to zero

the bifurcation to spatial patterns occurs at $q_a^0 = 1.008$. The coefficients that appear in the amplitude equation (34) are both negative: $\Re(X) < 0$, $\Re(Y) < 0$. Therefore, when $\nu = -1$, the curve $|\alpha|^2 = -\nu\Re(Y)/\Re(X) > 0$ is unstable, while $|\alpha| = 0$ is stable. Hence, the nonzero amplitude (the dashed line) bifurcates subcritically to the left. The analytical formula for amplitude $[\max(u) - \min(u)]$ is given in Appendix 3. In the next section, we perform numerical simulations to verify these analytical results.

Note that in this section, we have chosen the parameters to have different order of magnitudes (see, e.g., q_a and q_r). It is in this parameter regime that solutions become unstable, as predicted by the linear stability analysis.

4.2 Numerical results for a real bifurcation

To verify the results of this weakly nonlinear analysis, we perform numerical simulations. The numerical scheme we use is a second-order McCormack scheme [20]. The initial conditions are perturbations of the spatially homogeneous steady states (u^* , u^{**}). The amplitude of these perturbations is given by $0.02 \cos(k_c \pi x)$, $x \in [0, L]$.

Note that similar results can be obtained if we use random perturbations. For the parameter values specified in the previous section, the final heterogeneous pattern is similar to the one described in Fig. 2a. Figure 3 shows the amplitude of the total density, as determined by $\max(u^+ + u^-) - \min(u^+ + u^-)$. The solid circles represent the stable numerical solution, while the open circles represent the unstable numerical solution. For $q_a > q_a^0$, the spatially homogeneous steady state ($|\alpha| = 0$) bifurcates numerically to a large amplitude solution (solid circles). However, as we decrease q_a , we observe hysteresis behavior: the solution does not return to the spatially homogeneous steady state when $q_a = q_a^0$. It will eventually return to this steady state for some $q_a < q_a^0$. This is consistent with the previous analytical results regarding the existence of an unstable amplitude that bifurcates subcritically. We checked numerically the existence of this branch by choosing the initial conditions to be perturbations of the spatially homogeneous steady states with terms of the form $\hat{A} \cos(k_c \pi x)$, where \hat{A} is the variable amplitude. For $q_a < q_a^0$, the curve formed of open circles represents the unstable branch. This curve represents a threshold: perturbations with amplitude \hat{A} on or above this curve grow until the solution reaches the upper stable branch, whereas perturbations with amplitude below this curve decay to zero. Since the spatially homogeneous steady state is $(u_3^*, u_3^*) = (1, 1)$, imposing the condition that the initial solution is positive, forces us to use $\hat{A} \leq 2$. This happens for $q_a \in [0.915, 1.008]$.

There are two remarks regarding Fig. 3. First, it is known that for subcritical bifurcations, the cubic amplitude equation (34) can give only a qualitative description of the behavior of the solutions [10]. However, this qualitative behavior is enough for the biological questions we want to address in this paper. We note here that for $q_a < q_a^0$, the two unstable curves (the analytical and the numerical one) agree acceptably well, especially near the bifurcation point. Second, the high-amplitude solution drops to zero far from the bifurcation point (i.e., at $q_a = 0.83$). However, the weakly nonlinear analysis does not hold near the point where the solution drops to zero. Therefore, we do not expect here the stable high-amplitude curve and the unstable analytical curve to match. To study the behavior of the solution far from the bifurcation point, one can derive “phase equations” [33].

Figure 3 can be used to investigate the effect of attraction on the structure of stationary groups. Since the bifurcation is subcritical, the stable high-amplitude solution gives us the effect of the attractive interactions. More precisely, we notice that increasing the strength of the attraction (q_a) leads to larger amplitudes for the total density u . This means more compact groups. Moreover, for attraction less than q_a^0 , solutions with amplitude less than $\sqrt{-v\Re(Y)/\Re(X)}$ will decay. This suggests that groups that have a density less than a certain threshold will eventually disperse. Of course, this threshold depends not only on q_a , but also on all other parameters.

Note that the linear analysis predicted that the spatially homogeneous solution (i.e., the solution with zero amplitude) is stable for all $q_a < q_a^0$. The weakly nonlinear analysis, on the other hand, shows that it is only locally stable. The solution can be destabilized by perturbations with amplitudes larger than a certain threshold.

If we now consider $q_r = q_a = 0$ and large turning rates (λ_1, λ_2), we obtain similar results. However, in this case, the bifurcation parameter is the magnitude of alignment q_{al} . The final heterogeneous pattern is described in Fig. 2b. Figure 4

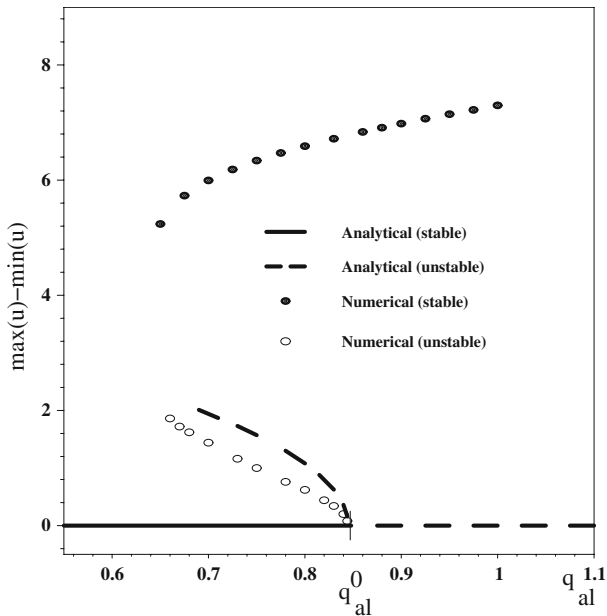


Fig. 4 The amplitude of the spatially heterogeneous solution $u(x, t) = u^+(x, t) + u^-(x, t)$ as we perturb the magnitude of alignment q_{al} . The *solid circles* represent the stable branch obtained numerically, while the *open circles* represent the unstable branch obtained numerically. The *dashed curve* represents the unstable branch obtained using weakly nonlinear analysis. For $q_{al} < q_{al}^0$, the zero amplitude branch (corresponding to $|\alpha^2| = 0$) is stable (the *continuous curve*). For $q_a > q_a^0$ it becomes unstable (the *dashed curve*). The parameters are: $q_{al}^0 = 0.845$, $k_c = k_{14} = 8.867$, $\lambda_1 = 2.0$, $\lambda_2 = 9.0$, $\gamma = 0.1$, $q_r = 0$, $q_a = 0$, $\gamma_0 = 2$

shows the amplitude of the stationary pattern that bifurcates subcritically to the left at $q_{al}^0 = 0.845$. Therefore, when the individual turning rates are very large, but at the same time organisms align with their neighbors, increasing the strength of alignment leads to higher amplitude solutions. Again, this means that the groups become more compact. Moreover, there is a similar threshold for the total density below which the groups will disperse. The existence of this threshold suggests that when individuals turn very frequently (i.e., $\lambda_{1,2}$ are large), the amplitude of the perturbations required to destabilize the spatially homogeneous solution decreases as alignment increases. Therefore, it seems that in this case, alignment is enough to cause aggregative behavior.

4.3 Weakly nonlinear analysis in the neighborhood of an imaginary bifurcation

In the following, we consider the case when the bifurcation to spatial heterogeneous patterns occurs at an imaginary eigenvalue. To keep the results tractable, we will assume that alignment is the only social interaction (that is, $q_a = q_r = 0$). This corresponds to the pattern shown in Fig. 3d. Consequently, we will fix all other parameters and assume that the bifurcation to spatially nonhomogeneous patterns occurs as q_{al} passes through a critical value q_{al}^0 . At the critical point (q_{al}^0, k_c) , the two

eigenvalues of the dispersion relation (7) are $\sigma_1(q_{al}^0, k_c) = i\omega$, and $\sigma_2(q_{al}^0, k_c) = \omega_0 + i\omega$, with $\omega_0 < 0$. As mentioned before, this happens when the spatially homogeneous steady state is any of the pairs (u_1^*, u_5^*) , or (u_5^*, u_1^*) . Throughout this subsection, we will assume that $(u^*, u^{**}) = (u_1^*, u_5^*)$ and study what happens in this case. Since the second eigenvalue has always a negative real part, we ignore it and focus only on the first eigenvalue. A solution of system (1) near the bifurcation point (q_{al}^0, k_c) has the form

$$u^\pm(x, t) \propto e^{i\omega t + ik_c x} + \text{c.c.} \quad (40)$$

As before, we perturb q_{al} away from the critical value q_{al}^0 ,

$$q_{al} = q_{al}^0 + \epsilon^2 v, \quad 0 < \epsilon \ll 1, \quad v = \pm 1. \quad (41)$$

Note that the spatially homogeneous steady state (u_3^*, u_3^*) , which we discussed in the previous section, does not depend on the bifurcation parameter. However, as shown in Fig. 1b and c, the spatially homogeneous steady state (u_1^*, u_5^*) does depend on the magnitude of alignment (q_{al}): as we increase q_{al} , u^* increases while u^{**} decreases. Therefore, in this case, a perturbation of q_{al} will induce a perturbation of these steady states:

$$u^* = u_0^* - \epsilon^2 v \left| \frac{du^*(q_{al}^0)}{dq_{al}} \right|, \quad u^{**} = u_0^{**} + \epsilon^2 v \left| \frac{du^*(q_{al}^0)}{dq_{al}} \right|, \quad (42)$$

where

$$\frac{\partial u^*(q_{al}^0)}{\partial q_{al}} = -\frac{M_5(u^{**} - u^*)}{L_1 + L_2 - 2q_{al}^0 M_5}, \quad (43)$$

and the constants L_1 , L_2 and M_5 are given by (8). For notational simplicity, we will drop the index “0” from the spatially homogeneous steady states u_0^* and u_0^{**} . Therefore, the left- and right-moving densities can be written as

$$\begin{aligned} u^+(x, t, \epsilon, T) &= u^* - \epsilon^2 v \left| \frac{du^*(q_{al}^0)}{dq_{al}} \right| + \epsilon u_1^+ + \epsilon^2 u_2^+ + \epsilon^3 u_3^+ + O(\epsilon^4), \\ u^-(x, t, \epsilon, T) &= u^{**} + \epsilon^2 v \left| \frac{du^*(q_{al}^0)}{dq_{al}} \right| + \epsilon u_1^- + \epsilon^2 u_2^- + \epsilon^3 u_3^- + O(\epsilon^4). \end{aligned} \quad (44)$$

Expanding the dispersion relation in power series leads to

$$\sigma(q_{al}, k_c) = \sigma(q_{al}^0, k_c) + \frac{\partial \sigma(q_{al}^0, k_c)}{\partial q_{al}} \epsilon^2 v + O(\epsilon^4). \quad (45)$$

To calculate the $O(\epsilon^2)$ term that appears in (45), we use (7):

$$\frac{\partial \sigma(q_{al}^0, k_c)}{\partial q_{al}} = \frac{-i\omega \frac{\partial C(q_{al}^0, k_c, u^*)}{\partial q_{al}} - \frac{\partial D(q_{al}^0, k_c, u^*)}{\partial q_{al}}}{2i\omega + C(q_{al}^0, k_c, u^*)}. \tag{46}$$

Because u^* and $u^{**} = A - u^*$ depend on q_{al} , the terms $\frac{\partial C}{\partial q_{al}}$ and $\frac{\partial D}{\partial q_{al}}$ are given in terms of the derivative of u^* with respect to q_{al} . Hence, when $\sigma(q_{al}^0, k_c) = i\omega$, we obtain

$$\frac{\partial \sigma}{\partial q_{al}} = \frac{-(u^{**} - u^*)P - M_7 \Delta - \frac{2q_{al}^0(u^{**} - u^*)M_5}{L_1 + L_2 - 2q_{al}^0 M_5} \left(P + \Delta(P_1 - P_2 - 4q_{al}^0(u^* S_1 - u^{**} S_2)) \right)}{2i\omega + L_1 + L_2 - M_5 q_{al}^0 (\hat{K}_{al}^+ + \hat{K}_{al}^-)}, \tag{47}$$

where

$$\begin{aligned} P &= P_1(i\omega - \gamma i k_c) - P_2(i\omega + \gamma i k_c), \\ \Delta &= \hat{K}_{al}^+(i\omega + \gamma i k_c) + \hat{K}_{al}^-(i\omega - \gamma i k_c), \\ M_7 &= M_5 + 2q_{al}^0(u^{**} - u^*)(u^* S_1 - u^{**} S_2), \end{aligned} \tag{48}$$

while the rest of the constants are given by (8).

Since the eigenvalues are imaginary, the spatially homogeneous steady states become unstable to *spatiotemporal patterns*, and therefore, the linear operator associated to system (1) is given by

$$L(\mathbf{u}) = \begin{pmatrix} \partial_t + \gamma \partial_x + L_1 + M_5 q_{al}^0 K_{al} * \cdot & -L_2 + M_5 q_{al}^0 K_{al} * \cdot \\ -L_1 - M_5 q_{al}^0 K_{al} * \cdot & \partial_t - \gamma \partial_x + L_2 - M_5 q_{al}^0 K_{al} * \cdot \end{pmatrix} \begin{pmatrix} u^+ \\ u^- \end{pmatrix}. \tag{49}$$

However, throughout the analysis, we will use L_{ω, k_c} which is obtained by applying the operator L to solutions of the form $e^{i\omega t + i k_c x}$:

$$L_{\omega, k_c} = \begin{pmatrix} i\omega + \gamma i k_c + L_1 - M_5 q_{al}^0 \hat{K}_{al}^- & -L_2 + M_5 q_{al}^0 \hat{K}_{al}^+ \\ -L_1 + M_5 q_{al}^0 \hat{K}_{al}^- & i\omega - \gamma i k_c + L_2 - M_5 q_{al}^0 \hat{K}_{al}^+ \end{pmatrix}. \tag{50}$$

The corresponding adjoint operator \bar{L}_{ω, k_c}^T is given in Appendix 4. Following the same steps as before, at $O(\epsilon^3)$ we have to impose the condition that the solution verifies the Fredholm Alternative. This leads to a similar amplitude equation,

$$\frac{d\alpha}{dT} = -\nu\alpha Y - \alpha|\alpha|^2 X, \tag{51}$$

where

$$Y = \frac{\bar{\mathbf{V}} \cdot \mathbf{R}^{(2)}}{\bar{\mathbf{V}} \cdot \mathbf{R}^{(3)}}, \quad X = \frac{\bar{\mathbf{V}} \cdot \mathbf{R}^{(1)}}{\bar{\mathbf{V}} \cdot \mathbf{R}^{(3)}}. \quad (52)$$

After some lengthy computations, we can verify that

$$Y = \frac{d\sigma(q_{al}^0)}{dq_{al}}, \quad (53)$$

with $\frac{d\sigma}{dq_{al}}$ given by (47). Therefore the linear approximation of this amplitude equation agrees with the linear prediction given by the dispersion relation (45).

Similar to the results in Sect. 4.2, the steady-state solutions for the magnitude of the amplitude equation are given by

$$|\alpha| = 0, \quad |\alpha| = \sqrt{-\nu \Re(Y) / \Re(X)}. \quad (54)$$

The zero state $|\alpha| = 0$ is stable if $\nu \Re(Y) > 0$, and unstable otherwise. The state $|\alpha| = \sqrt{-\nu \Re(Y) / \Re(X)}$ is unstable if $\nu \Re(Y) > 0$, and stable otherwise.

For $q_r = q_a = 0$, $\lambda_1 = 0.2/0.7$, $\lambda_2 = 0.9/0.7$, $\gamma = 0.1$, and $k_c = k_{17} = 10.55$, the two coefficients that appear in (54) are $\Re(Y) > 0$ and $\Re(X) < 0$. Hence $|\alpha|^2 = -\nu \frac{\Re(Y)}{\Re(X)} > 0$ if $\nu > 0$, which means that solution bifurcates to the right. Moreover, since $\nu \Re(Y) > 0$, the zero-amplitude steady state is stable, whereas the nonzero-amplitude solution is unstable. Figure 5 shows this bifurcation. The continuous curve represents the stable solution, whereas the dashed curve represents the unstable solution obtained using weakly nonlinear analysis.

4.4 Numerical results for the imaginary bifurcation

To confirm the validity of these results, we perform numerical simulations. Again, the initial conditions are perturbations of the spatially homogeneous steady states with terms of the form $\hat{A} \cos(k_c \pi x)$. Figure 5 shows the amplitude of the spatiotemporal solutions as we perturb the magnitude of alignment q_{al} . As before, the spatial homogeneous solution bifurcates subcritically to spatial heterogeneous solutions represented by the traveling trains (seen in Fig. 3d). The solid circles represent the stable numerical solution, while the open circles represent the unstable numerical solution. For $q_{al} \geq q_{al}^0$, the branch described by the open circles represents a threshold: perturbations with amplitude below this curve decay to zero, while perturbations with amplitude on or above this curve grow to the upper branch. Therefore, the numerical results are consistent with the analytical results.

We notice that increasing the magnitude of alignment leads to a slight decrease in the amplitude of the solutions. This suggests that moving groups become more elongated, as alignment is increased. This is opposite to the effect observed in the case of stationary groups. There, the alignment makes the group more compact. As before, there is a certain threshold for the total density, corresponding to $|\alpha|^2 = -\nu \frac{\Re(Y)}{\Re(X)}$. Groups

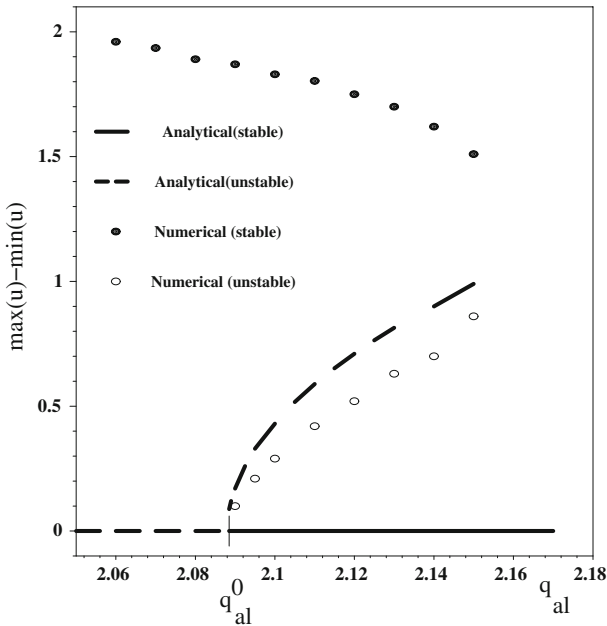


Fig. 5 Amplitude of the spatially heterogeneous solution as we perturb the magnitude of alignment q_{al} . The *solid circles* represent the stable numerical solution, while the *open circles* represent the unstable numerical solution. The *continuous curve* represents the stable analytical solution, while the *dashed curve* represents the unstable analytical solution. The critical value of q_{al} is $q_{al}^0 = 2.088$. The other parameters are: $\lambda_1 = 0.2/0.7$, $\lambda_2 = 0.9/0.7$, $\gamma = 0.1$, $q_r = q_a = 0$, $L = 10.12$, $k_c = 10.55$, $\gamma_0 = 2$

with total density greater than this threshold will become more dense and persist for a long time, while groups with the density below this threshold will disperse. Moreover, the existence of this threshold suggests that when individuals do not turn very frequently (i.e., $\lambda_{1,2}$ are small), the amplitude of the perturbations required to destabilize the homogeneous solution increases as alignment increases. This is opposite to the case discussed in Sect. 4.2. Here, alignment is not enough to cause aggregative behavior. It requires a certain amount of noise (i.e., perturbations), which combined with alignment, would lead to the formation of groups.

As mentioned in Sect. 3, introducing attractive and repulsive interactions leads to the emergence of the first wave number, k_1 , as shown in Fig. 2c. In this case, the result is a traveling train formed only of one group (see Fig. 2c). Figure 6 shows the subcritical bifurcation obtained in this case. The stable high-amplitude branch (the solid circles) corresponds to the solution shown in Fig. 2c. The effect of alignment on the moving group is similar to the previous case.

5 Discussion

In this article, we have analyzed two spatial and spatiotemporal patterns displayed by a hyperbolic model used to study animal group formation. The investigated patterns are

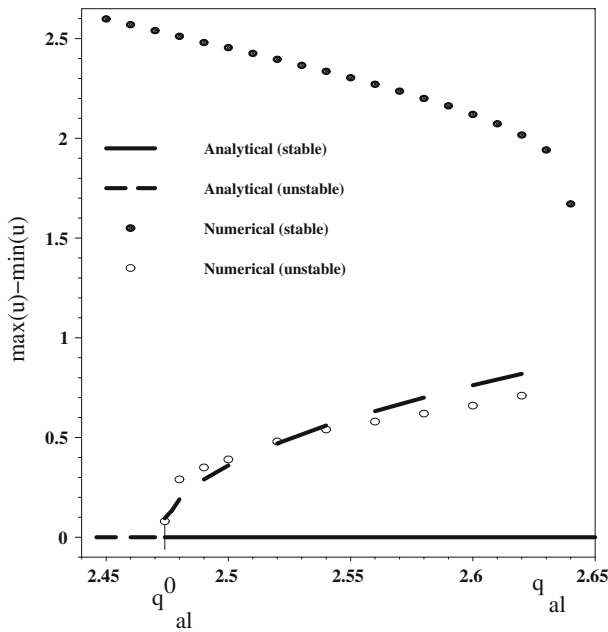


Fig. 6 The amplitude of the spatially heterogeneous solution as we perturb the magnitude of alignment q_{al} , while taking into consideration the attractive and repulsive interactions. The *solid circles* represent the stable numerical solution, while the *open circles* represent the unstable numerical solution. The *dashed curves* represent the unstable analytical solution. The critical value of q_{al} is $q_{al}^0 = 2.472$. The other parameters are: $\lambda_1 = 0.2$, $\lambda_2 = 0.9$, $\gamma = 0.1$, $q_r = 0.1$, $q_a = 1.0$, $L = 10$, $k_c = 0.628$, $\gamma_0 = 2$

stationary pulses and traveling trains. Using a weakly nonlinear analysis, we show that the stationary pulses arise through a real bifurcation from the spatially homogeneous steady state (u_3^*, u_3^*) . The traveling trains arise through an imaginary bifurcation from a different steady state, namely (u_1^*, u_5^*) . In both cases, the bifurcations are subcritical. It should be mentioned that while the steady state (u_3^*, u_3^*) is constant, the steady state (u_1^*, u_5^*) depends on the bifurcation parameter.

Note that the linear stability analysis predicts that in some parameter spaces, the spatially homogeneous steady states are stable to infinitesimal disturbances (see, e.g., Fig. 4, for $q_{al} < q_{al}^0$). However, the weakly nonlinear theory shows that these steady states can actually become unstable to disturbances whose amplitudes are greater than a threshold which corresponds to $|\alpha|^2 = -\nu \frac{\Re(Y)}{\Re(X)}$. Moreover, the weakly nonlinear analysis helps us understand some aspects of the complex structure of the attractors of the system. Figure 5, e.g., shows that for $q_{al} \in (2.088, 2.15)$ there is a locally stable spatially homogeneous steady state (u_1^*, u_5^*) , surrounded by an unstable limit cycle. This unstable limit cycle is then surrounded by another stable limit cycle. It is precisely this stable limit cycle which attracts the solutions obtained by perturbing the steady states (u_2^*, u_4^*) . Moreover, this limit cycle attracts large amplitude perturbations of the locally stable spatially homogeneous steady states (u_3^*, u_3^*) (see Fig. 1c).

In Sect. 4, we mentioned that the traveling pulses which can be observed in this hyperbolic system, occur far from the bifurcation point. They are actually secondary

bifurcations which arise from traveling trains when alignment (q_{al}) and the inter-individual attraction (q_a) are sufficiently large. The semi-zigzag pulses are a transient pattern determined by secondary symmetry-breaking bifurcations which cause the transition from traveling trains to stationary pulses. They occur in a parameter space far from the bifurcation point, when two adjacent wave numbers interact with each other. The investigation of these patterns is a subject for further research.

Note that there are other symmetries involved in the emergence of different patterns, and which correspond to particular parameter subspaces. For example, when $q_a = q_r = 0$, the time-independent solutions (i.e., $u_t^\pm = 0$) are invariant under the transformation $(u^+(x), u^-(x)) \rightarrow (u^-(-x), u^+(-x))$. When $q_{al} = 0$, the time-independent solutions are invariant under the transformation $(u^+(x), u^-(x)) \rightarrow (-u^-(-x), -u^+(-x))$. Moreover, in different parameter spaces it is possible to have mode interactions (not discussed here): steady-state/Hopf interactions, and Hopf/Hopf interactions. The complexity of all these symmetries suggests that, even if the weakly nonlinear results are very useful, we are still far from thoroughly understanding all these patterns.

Before discussing the biological implications of the weakly nonlinear results, we should stress the fact that the one-dimensional patterns investigated in the previous sections can approximate the behavior of animal groups that move through a domain which is much longer than wide. Therefore, the biological insights obtained using weakly nonlinear analysis are valid only under these assumptions. However, in nature, the majority of the aggregations are in two and three dimensions. The rigorous analysis of the social interactions that lead to the formation of these aggregations requires a model which is two- or three-dimensional. A two-dimensional analogue of system (1) can be derived using a velocity-jump process (see, e.g., [36, 38]). We briefly describe such a model in Appendix 1. A detailed description and analysis of this two-dimensional model is beyond the scope of this paper. However, we would expect more spatial and spatiotemporal patterns compared to the one-dimensional case. The patterns are determined by the symmetries of the system, and in particular of the interaction kernels, and they can be described in terms of the competition between odd and even wave numbers (see also [3, 4] for the treatment of a nonlocal two-dimensional problem).

Note that for the one-dimensional model, as well as for the two-dimensional analogue, the symmetries of the system can restrict the form of the solutions, and the amplitude equations (see, e.g., [17] for a general discussion on the subject, and [8] for the description of ten generic instabilities of a one-dimensional model).

Returning now to the results obtained through weakly nonlinear analysis, it is known that for subcritical bifurcations, the unstable branch obtained using a cubic amplitude equation gives only qualitative information about the solution [10]. A more accurate result can be obtained by adding higher-order terms to obtain a quintic amplitude equation. Moreover, far from the bifurcation point, one can only derive “phase equations” to study the behavior of the solution. However, due to the complexity of our system, as well as the type of questions we are addressing (that is, the effect of the social interactions on the amplitude of spatial and spatiotemporal patterns), it is sufficient to derive a cubic amplitude equation.

We used the bifurcation diagrams for the amplitude of the solutions to study the effect of social interactions on the structure of the aggregations. As expected, increasing inter-individual attraction leads to more compact stationary groups. This kind

of behavior can be observed in schools of fish [6,42], when a nearby predator leads to increased attraction towards neighbors which causes the group to form very tight stationary aggregations. Alignment on the other hand, has dual effects, depending on whether the group is stationary or moving. We have seen that in the case of stationary groups with high individual turning rates, alignment has an aggregative effect, with the groups becoming more dense. However, in case of moving groups, the effect of alignment is opposite: the density decreases as the groups become more elongated. When alignment becomes very large, the groups disintegrate. Similar results regarding this effect of alignment on moving groups were obtained with individual based models [29].

Moreover, the bifurcation diagrams show that there is a competition between the turning behavior and the magnitude of the alignment interaction that leads to the formation of stable aggregations. For example, in case of high turning rates the amplitude of the perturbation required to destabilize the homogeneous solution decreases as alignment increases. In case of low turning rates, the situation is opposite: the amplitude of the required perturbations decreases as alignment increases.

The subcritical bifurcation suggests that there is a threshold group density, such that groups with densities below this threshold will disperse, while groups with densities above this threshold will become even more dense and persist for a longer time. This transition between the disordered behavior represented here by the homogeneous solution, and the ordered behavior represented by the high-density stationary or moving groups, is particularly important for the area of animal group formation and movement. It is known that some insect species (such as ants [2], or locusts [5]) exhibit transitions between disordered and ordered activity behaviors, and these transitions depend on animal density. For example, Buhl et al. [5] have shown experimentally and numerically (using an individual-based model) that as the density of locusts in a group increases, there is a transition from disordered movement to collective motion of aligned groups. Understanding such transitions has potential applications to understanding and controlling the outbreaks of different insect pests, such as locusts.

In this paper, we have analyzed the patterns displayed by only one of the five submodels described in [13]. It is possible that other patterns, corresponding to the other four submodels, arise through supercritical bifurcations. However, this aspect has not yet been investigated. Still, we can conclude that the subcritical bifurcations seem to play an important role in the understanding of the effects of biological parameters to the formation and persistence of certain animal groups (such as insects). A supercritical bifurcation (i.e., bifurcation to a small, stable, amplitude solution) would suggest that increasing a certain parameter would lead to the formation of denser, well coordinated groups. This may be the case for some animal groups, but not necessarily for insects like locusts or ants. A subcritical bifurcation, on the other hand, suggests the existence of a density threshold below which well coordinated groups cannot persist. Moreover, this type of bifurcation helps us connect the threshold for the total animal density to different behaviors. More precisely, this threshold depends on different parameter values which characterize different group behaviors.

To summarize, the results presented in this article are a first attempt to understand the effects of the nonlocal social interactions on the resulting group patterns. Due to the complexity of this model, we are still far from completely understanding the dynamics of this hyperbolic system.

Acknowledgments RE would like to thank F. Lutscher for fruitful discussions regarding the existence of solutions, and J. M. Lee for discussions regarding the numerical scheme. RE acknowledges support from University of Alberta Queen Elizabeth II Scholarship (Doctoral). GdeV acknowledges partial support from an NSERC Discovery Grant. MAL acknowledges support from an NSERC Discovery Grant and Canada Research Chair.

Appendix 1: Model extension in two dimensions

A two-dimensional analogue of system (1) can be derived using a velocity-jump process (see, e.g., [36, 38]):

$$\partial_t u + \gamma e^{i\phi} \nabla_x u = -\lambda(x, \phi, t)u + \int \lambda(x, \phi', t)T(\phi, \phi')u(x, \phi', t)d\phi'. \quad (55)$$

Here u is the total density, $\lambda(x, \phi, t)$ is the probability that a reorientation occurs at (x, ϕ, t) , and $T(\phi, \phi')$ is the probability of choosing ϕ' the new direction, provided that a reorientation occurs. These last two terms, $\lambda(x, \phi, t)$, and $T(\phi, \phi')$, are determined by the assumptions we make about the communication mechanisms. Following the same procedure as in [38], we can define

$$\lambda(x, \phi, t) = \lambda_1 + \lambda_2 h \left(\int_0^{2\pi} \int_{\|s-x\| \leq s_r} K_r(D_\phi(s-x), \theta - \phi) ds d\theta \right. \\ \left. + \int_0^{2\pi} \int_{\|s-x\| \leq s_a} K_a(D_\phi(s-x), \theta - \phi) ds d\theta \right. \\ \left. + \int_0^{2\pi} \int_{\|s-x\| \leq s_{al}} K_{al}(D_\phi(s-x), \theta - \phi) ds d\theta \right), \quad (56)$$

and

$$T(\phi, \phi') = \int_0^{2\pi} \int_{\|s-x\| \leq s_r} \bar{K}_r(D_\phi(s-x), \theta - \phi, \phi' - \phi) ds d\theta \\ + \int_0^{2\pi} \int_{\|s-x\| \leq s_a} \bar{K}_a(D_\phi(s-x), \theta - \phi, \phi' - \phi) ds d\theta \\ + \int_0^{2\pi} \int_{\|s-x\| \leq s_{al}} \bar{K}_{al}(D_\phi(s-x), \theta - \phi, \phi' - \phi) ds d\theta + T_0(\phi' - \phi) \quad (57)$$

Here D_ϕ denotes the matrix

$$D_\phi = \begin{pmatrix} \cos(\phi) & \sin(\phi) \\ -\sin(\phi) & \cos(\phi) \end{pmatrix}, \quad (58)$$

The kernels $K_i(D_\phi(s-x), \theta - \phi) > 0$, $i = r, a, al$, with $\int_D K_i(D_\phi(s-x), \theta - \phi) d\theta = 1$, describe the repulsive, attractive, and alignment interactions that trigger the turning. The kernels $\bar{K}_i(D_\phi(s-x), \theta - \phi, \phi' - \phi) > 0$, $i = r, a, al$, describe the social interactions that lead to the probability of choosing the new direction ϕ' . If there are no individuals within the perception range, the new direction is given by $T_0(\phi' - \phi)$. The kernels \bar{K}_i and T_0 satisfy

$$\int_0^{2\pi} \bar{K}_i(\cdot, \cdot, \phi) d\phi = 0, \quad \int_0^{2\pi} T_0(\phi) d\phi = 1. \quad (59)$$

The definition of these kernels depends on the assumptions we make about the different communication mechanisms that take place in two dimensions.

To reduce this model to the previous one-dimensional case, we choose $\phi = \pm \frac{\pi}{2}$. In this case, the turning rates can be written as

$$\begin{aligned} \Lambda^+ = h & \left(\int_{\|\bar{x}-x\|} K_r \left(D_{\frac{\pi}{2}}(s-x), 0 \right) u \left(s, \frac{\pi}{2}, t \right) \right. \\ & - K_r \left(D_{\frac{\pi}{2}}(s-x), -\pi \right) u \left(s, -\frac{\pi}{2}, t \right) ds \\ & + \int_{\|\bar{x}-x\|} K_a \left(D_{\frac{\pi}{2}}(s-x), 0 \right) u \left(s, \frac{\pi}{2}, t \right) \\ & - K_a \left(D_{\frac{\pi}{2}}(s-x), -\pi \right) u \left(s, -\frac{\pi}{2}, t \right) ds \\ & + \int_{\|\bar{x}-x\|} K_{al} \left(D_{\frac{\pi}{2}}(s-x), 0 \right) u \left(s, \frac{\pi}{2}, t \right) \\ & \left. - K_{al} \left(D_{\frac{\pi}{2}}(s-x), -\pi \right) u \left(s, -\frac{\pi}{2}, t \right) ds \right), \quad (60) \end{aligned}$$

$$\begin{aligned} \Lambda^- = h & \left(\int_{\|\bar{x}-x\|} K_r \left(D_{-\frac{\pi}{2}}(s-x), -\pi \right) u \left(s, -\frac{\pi}{2}, t \right) \right. \\ & - K_r \left(D_{-\frac{\pi}{2}}(s-x), 0 \right) u \left(s, \frac{\pi}{2}, t \right) ds \end{aligned}$$

$$\begin{aligned}
 &+ \int_{\|\bar{x}-x\|} K_a \left(D_{-\frac{\pi}{2}}(s-x), -\pi \right) u \left(s, -\frac{\pi}{2}, t \right) \\
 &- K_a \left(D_{-\frac{\pi}{2}}(s-x), 0 \right) u \left(s, \frac{\pi}{2}, t \right) ds \\
 &+ \int_{\|\bar{x}-x\|} K_{al} \left(D_{-\frac{\pi}{2}}(s-x), -\pi \right) u \left(s, -\frac{\pi}{2}, t \right) \\
 &- K_{al} \left(D_{-\frac{\pi}{2}}(s-x), 0 \right) u \left(s, \frac{\pi}{2}, t \right) ds \Big). \tag{61}
 \end{aligned}$$

Let $u^+(s, t) = u(s, \frac{\pi}{2}, t)$, and $u^-(s, t) = u(s, -\frac{\pi}{2}, t)$. Depending on the assumptions we make about the kernels $K_i, i = r, a, al$, we can recover the different communication mechanisms introduced in [13]. For example, if $K_i(y, 0) = 0, K_i(y, -\pi) = -K_i(y, \pi), \bar{K}_i \equiv 0$, and $T_0(\pm\frac{\pi}{2}) = 1$, we can recover the communication mechanism corresponding to model *M5*. If $K_i(y, 0) = K_i(y, -\pi) \neq 0, \bar{K}_i \equiv 0$, and $T_0(\pm\frac{\pi}{2}) = 1$, we can recover the mechanism corresponding to model *M4*.

This reduction of the model suggests that some of the solutions of the one-dimensional system can be thought as special solutions of the two-dimensional model. However, a detailed description and analysis of this two-dimensional model is the subject of future research.

Appendix 2: Existence of solutions for the hyperbolic system

The proof for the existence of solutions of system (1) uses the characteristic equations of the hyperbolic system (1):

$$\frac{d\zeta^+}{ds} = \gamma, \quad \frac{d\zeta^-}{ds} = -\gamma. \tag{62}$$

We denote $\zeta^\pm = \Xi^\pm(s; x, t)$ as the solution of this ODE system, passing through the point (x, t) . If we set $U^\pm(s) = u(\Xi^\pm(s; x, t), s)$, we can rewrite the hyperbolic system (1) as:

$$\begin{aligned}
 \frac{dU^+}{dt}(s; x, t) &= -\lambda^+(U^+(s), U^-(s))U^+(s) + \lambda^-(U^+(s), U^-(s))U^-(s), \\
 \frac{dU^-}{dt}(s; x, t) &= \lambda^+(U^+(s), U^-(s))U^+(s) - \lambda^-(U^+(s), U^-(s))U^-(s).
 \end{aligned} \tag{63}$$

Integrating (63) along the characteristics gives

$$U^+(\zeta^+) = U^+(\zeta_0) + \int_{\zeta_0}^{\zeta^+} (-\lambda^+(U^+, U^-)U^+ + \lambda^+(U^+, U^-)U^-) (y)dy, \tag{64}$$

$$U^-(\zeta^-) = U^-(\zeta_0) + \int_{\zeta_0}^{\zeta^-} (\lambda^+(U^+, U^-)U^+ - \lambda^-(U^+, U^-)U^-) (y) dy. \quad (65)$$

Note that, a pair of functions (u^+, u^-) which satisfies (64) and (65) is called a *mild solution* of system (1).

We define the operator $G(U^+, U^-) = (G_1(U^+, U^-), G_2(U^+, U^-))$, where G_1 and G_2 are described by the two expressions on the right hand side of (64) and (65), respectively. Then, finding a unique mild solution of (1) reduces to finding a fixed point of the map $(U^+, U^-) \mapsto G(U^+, U^-)$.

To prove the existence of a unique weak solution $u^\pm \in L^\infty(\mathbf{R} \times [0, \infty))$ of system (1), let us consider the Banach spaces $X := L^\infty(\mathbf{R} \times [0, t_0))$ with norm $\|u\|_X := \sup \|u(\cdot, t)\|_\infty$, and $\bar{X} := L^\infty(\mathbf{R})$. On $X \times X$ we have the norm $\|(u, v)\|_{X \times X} := \max(\|u\|_X, \|v\|_X)$. We also define $B = B(R, X) := \{u \in X : \|u(x, t)\|_X \leq R\}$.

Following the same steps as in [22, 25], for all $\omega \in X$, with $\omega^\pm(0, \cdot) = u_0^\pm \in L^\infty(R)$, we consider the Cauchy problem

$$\begin{aligned} u_t^+ + \gamma u_x^+ &= -\lambda^+(\omega^+, \omega^-)\omega^+ + \lambda^-(\omega^+, \omega^-)\omega^-, \\ u_t^- - \gamma u_x^- &= \lambda^+(\omega^+, \omega^-)\omega^+ - \lambda^-(\omega^+, \omega^-)\omega^-, \\ u^\pm(0, x) &= u_0^\pm(x). \end{aligned} \quad (66)$$

We prove that the operator G defined by (64) and (65) is a contraction:

1. $G : X_R \times X_R \mapsto X_R \times X_R$ (where X_R is a closed subset of Banach space X)
2. For $(\omega^+, \omega^-), (\theta^+, \theta^-) \in X_R \times X_R$, and $0 < \epsilon < 1$,

$$\|G(\omega^+, \omega^-) - G(\theta^+, \theta^-)\|_{X_R \times X_R} \leq \epsilon \|(\omega^+, \omega^-) - (\theta^+, \theta^-)\|_{X_R \times X_R}.$$

To prove that G maps a closed subset of a Banach space into itself, we only have to assume that u_0^\pm is bounded in $\|\cdot\|_{X_R}$ by a constant M^* . We then choose $R \geq M^* + \epsilon_1$, for some $\epsilon_1 > 0$. For $(\omega^+, \omega^-) \in B$, with $\omega^\pm(0, \cdot) = U_0^\pm$, we have

$$\begin{aligned} \|G_1(\omega^+, \omega^-)\|_X &\leq \|U_0^\pm\|_{\bar{X}} + \int_{\zeta_0}^{\zeta^+} \|(-\lambda^+(\omega^+, \omega^-)\omega^+ + \lambda^-(\omega^+, \omega^-)\omega^-) (y)\|_X dy \\ &\leq M^* + \gamma t_0 R (\sup_B \lambda^+(\omega^+, \omega^-) + \sup_B \lambda^-(\omega^+, \omega^-)). \end{aligned}$$

Let $K = \sup_B \lambda^+(\omega^+, \omega^-) + \sup_B \lambda^-(\omega^+, \omega^-)$, and choose $t_0 \leq \frac{\epsilon_1}{\gamma R K} = T_1$ to obtain the bound $\|G_1(\omega^+, \omega^-)\|_X \leq M^* + \epsilon_1 \leq R$. A similar result holds for G_2 .

To prove the contraction condition, let us consider $(\omega^+, \omega^-), (\theta^+, \theta^-) \in B$, with $\omega^\pm(0, \cdot) = \theta^\pm(0, \cdot) = U_0^\pm$. Then,

$$\begin{aligned}
& \|G_1(\omega^+, \omega^-) - G_1(\theta^+, \theta^-)\|_{X \times X} \\
&= \left\| \int_{\xi_0}^{\xi^+} (\lambda^+(\theta^+, \theta^-)\theta^+ - \lambda^+(\omega^+, \omega^-)\omega^+ \right. \\
&\quad \left. + \lambda^-(\omega^+, \omega^-)\omega^- - \lambda^-(\theta^+, \theta^-)\theta^-) (y) dy \right\|_X \\
&= \frac{1}{2} \left\| - \int_{\xi_0}^{\xi^+} (\lambda^+(\omega^+, \omega^-) + \lambda^+(\theta^+, \theta^-)) (\omega^+ - \theta^+)(y, t) dy \right. \\
&\quad \left. + \int_{\xi_0}^{\xi^+} (\lambda^-(\omega^+, \omega^-) + \lambda^-(\theta^+, \theta^-)) (\omega^- - \theta^-)(y, t) dy \right. \\
&\quad \left. + \int_{\xi_0}^{\xi^+} (\lambda^+(\theta^+, \theta^-) - \lambda^+(\omega^+, \omega^-)) (\omega^+ + \theta^+)(y, t) dy \right. \\
&\quad \left. - \int_{\xi_0}^{\xi^+} (\lambda^-(\theta^+, \theta^-) - \lambda^-(\omega^+, \omega^-)) (\omega^- + \theta^-)(y, t) dy \right\|_X. \quad (67)
\end{aligned}$$

We assumed that the turning rates are locally Lipschitz continuous as functions of y^\pm . Let L^\pm be the Lipschitz constants. Using (2), we obtain

$$\begin{aligned}
& \|\lambda^\pm(\omega^+, \omega^-) - \lambda^\pm(\theta^+, \theta^-)\|_{X \times X} \\
&= \|h(y^\pm(\omega^+, \omega^-)) - h(y^\pm(\theta^+, \theta^-))\|_{X \times X} \\
&\leq L^\pm(R) \|y^\pm(\omega^+, \omega^-) - y^\pm(\theta^+, \theta^-)\|_{X \times X} \\
&= L^\pm(R) \left\| \int_0^\infty (\pm q_r K_r(s) \mp q_a K_a(s)) (\omega(x \pm s, t) - \theta(x \pm s, t) - \omega(x \mp s, t) \right. \\
&\quad \left. + \theta(x \mp s, t)) ds \pm \int_0^\infty q_{al} K_{al}(s) (\omega^-(x + s, t) - \theta^-(x + s, t) - \omega^+(x - s) \right. \\
&\quad \left. + \theta^+(x - s)) ds \right\|_X \\
&\leq L_{1,2}(R) \max(\|\omega^+ - \theta^+\|_X, \|\omega^- - \theta^-\|_X) \\
&= L_{1,2}(R) \|(\omega^+, \omega^-) - (\theta^+, \theta^-)\|_{X \times X}. \quad (68)
\end{aligned}$$

Here $L_{1,2}(R) = L^\pm(R)C(q_r, q_a, q_{al})$, where $C(q_r, q_a, q_{al})$ is a constant that depends on the magnitudes of the social interactions. Hence, λ^\pm are locally Lipschitz continuous as functions of ω^\pm, θ^\pm , with $L_1(R)$ and $L_2(R)$ the Lipschitz constants. We therefore have

$$\begin{aligned} & \|G_1(\omega^+, \omega^-) - G_1(\theta^+, \theta^-)\|_{X \times X} \\ & \leq \frac{1}{2} |\zeta^+ - \zeta_0| 2\sup_B \lambda^+(\omega^+, \omega^-) \|\omega^+ - \theta^+\|_X \\ & \quad + \frac{1}{2} |\zeta^+ - \zeta_0| 2\sup_B \lambda^-(\omega^+, \omega^-) \|\omega^- - \theta^-\|_X \\ & \quad + \frac{1}{2} |\zeta^+ - \zeta_0| \|\omega^+ + \theta^+\|_X L_1(R) \max(\|\theta^+ - \omega^+\|_X, \|\theta^- - \omega^-\|_X) \\ & \quad + \frac{1}{2} |\zeta^+ - \zeta_0| \|\omega^- + \theta^-\|_X L_2(R) \max(\|\theta^+ - \omega^+\|_X, \|\theta^- - \omega^-\|_X). \end{aligned} \quad (69)$$

Since $\|\omega^\pm + \theta^\pm\|_X \leq 2R$, we obtain

$$\begin{aligned} \|G_1(\omega^+, \omega^-) - G_1(\theta^+, \theta^-)\|_{X \times X} & \leq \gamma t_0 (K + L_1(R)R \\ & \quad + L_2(R)R) \|(\omega^+, \omega^-) - (\theta^+, \theta^-)\|_{X \times X}. \end{aligned} \quad (70)$$

Let us define $T_2 = \frac{\epsilon_2}{\gamma(K + L_1(R)R + L_2(R)R)}$, for some $\epsilon_2 > 0$, and choose $t_0 \leq T_2$. We then obtain

$$\|G_1(\omega^+, \omega^-) - G_1(\theta^+, \theta^-)\|_{X \times X} \leq \epsilon_2 \|(\omega^+, \omega^-) - (\theta^+, \theta^-)\|_{X \times X}. \quad (71)$$

A similar estimate holds for G_2 . Then, for $t_0 \leq \min(T_1, T_2)$ we have

$$\|G(\omega^+, \omega^-) - G(\theta^+, \theta^-)\|_{X \times X} \leq \epsilon \|(\omega^+, \omega^-) - (\theta^+, \theta^-)\|_{X \times X}, \quad (72)$$

which implies that G is a contraction. Therefore, G has a unique fixed point $(u^+, u^-) \in X \times X$. Replacing ω^\pm in (64) and (65) with U^\pm results in:

$$\begin{aligned} \|U^+(\zeta^+)\|_X & \leq \|U^+(\zeta_0)\|_{\bar{X}} + \left\| \int_{\zeta_0}^{\zeta^+} (-\lambda^+(U^+, U^-)U^+ + \lambda^-(U^+, U^-)U^-)(y) dy \right\|_X, \\ \|U^-(\zeta^-)\|_X & \leq \|U^-(\zeta_0)\|_{\bar{X}} + \left\| \int_{\zeta_0}^{\zeta^-} (\lambda^+(U^+, U^-)U^+ - \lambda^-(U^+, U^-)U^-)(y) dy \right\|_X, \end{aligned}$$

and therefore,

$$\begin{aligned} \|U^+\|_X + \|U^-\|_X & \leq \|u_0^+\|_{\bar{X}} + \|u_0^-\|_{\bar{X}} \\ & \quad + 2\gamma t_0 (K + (L_1(R) + L_2(R))R) (\|U^+\|_X + \|U^-\|_X). \end{aligned} \quad (73)$$

Hence

$$\|U^+\|_X + \|U^-\|_X \leq \frac{1}{1-\epsilon} (\|U_0^+\|_{\bar{X}} + \|U_0^-\|_{\bar{X}}), \tag{74}$$

which implies that $u^\pm \in L^\infty(\mathbf{R} \times [0, t_0])$.

To prove the solution is defined for all time, it is enough to show that $\|U^\pm\|_X$ are bounded on any bounded interval $[0, T]$:

$$\begin{aligned} \frac{d}{ds} \|U^\pm(s, \cdot)\|_{L^\infty(\mathbf{R})} &\leq \left\| \frac{d}{ds} U^\pm(s, \cdot) \right\|_{L^\infty(\mathbf{R})} \\ &\leq \|\lambda^+(U^+, U^-)U^+\|_{L^\infty(\mathbf{R})} + \|\lambda^-(U^+, U^-)U^-\|_{L^\infty(\mathbf{R})} \\ &\leq M_2(\|U^+\|_{L^\infty(\mathbf{R})} + \|U^-\|_{L^\infty(\mathbf{R})}), \end{aligned} \tag{75}$$

where M_2 is the upper bound for λ^\pm . Therefore

$$\|U^+\|_{L^\infty(\mathbf{R})} + \|U^-\|_{L^\infty(\mathbf{R})} \leq (\|U_0^+\|_{L^\infty(\mathbf{R})} + \|U_0^-\|_{L^\infty(\mathbf{R})})e^{M_2s}. \tag{76}$$

Since $U^\pm(t, \cdot)$ are bounded on any bounded interval $[0, T]$, the solution exists for all time. □

Note that on a bounded domain $\Omega = [0, L]$, if we assume that the initial data $u_0^\pm(x)$ is periodic, then the mild solution $u^\pm(x, t) \in L^\infty(\Omega \times [0, \infty))$ is periodic.

We should also mention that since $\frac{d}{dt} \int_{-\infty}^{\infty} (u^+(x, t) + u^-(x, t))dx = 0$, it follows that if the initial condition satisfies $u_0^\pm \in L^1(\mathbf{R})$, then $u^\pm \in L^1(\mathbf{R})$.

Appendix 3: Detailed calculations for the weakly nonlinear analysis in the neighborhood of a real bifurcation

At $O(\epsilon)$, we calculate u_1^+ and u_1^- from

$$L(\mathbf{u}_1) = 0, \tag{77}$$

where $\mathbf{u}_1 = (u_1^+, u_1^-)^T = \alpha(T)\mathbf{v}e^{ikc x} + \text{c.c.}$, with $\mathbf{v} = (v_1, v_2)^T$, and ‘‘c.c.’’ denoting the complex conjugate terms. The components v_1 and v_2 are given by:

$$v_1 = \frac{L_1 - M_5\hat{K}^+}{\gamma ik + L_1 + M_5\hat{K}^+}, \quad v_2 = 1. \tag{78}$$

Here $\mathbf{E}_1 = \mathbf{N}_1 = 0$. At $O(\epsilon^2)$, the nonlinear terms are $\mathbf{E}_2 = 0$, and

$$\mathbf{N}_2 = \begin{pmatrix} u_1^+ P_1 K * u_1 + u_1^- P_1 K * u_1 \\ -u_1^+ P_1 K * u_1 - u_1^- P_1 K * u_1, \end{pmatrix}, \tag{79}$$

where $K = q_r(\tilde{K}_r - K_r) - q_a^0(\tilde{K}_a - K_a)$, and $\tilde{K}_{r,a}(s) = K_{r,a}(-s)$. Actually, \mathbf{N}_2 can be rewritten as

$$\mathbf{N}_2 = \alpha^2(T)e^{2ik_c x} \mathbf{Q}^{(1)} + |\alpha|^2 \mathbf{Q}^{(2)} + \text{c.c.}, \quad (80)$$

with $\mathbf{Q}^{(1)} = (Q_1^{(1)}, Q_2^{(1)})^T$ and $\mathbf{Q}^{(2)} = (Q_1^{(2)}, Q_2^{(2)})^T$. Equation $L(\mathbf{u}_2) + \mathbf{N}_2 = 0$ is then solved for $\mathbf{u}_2 = (u_2^+, u_2^-)^T$, where

$$\mathbf{u}_2 = \alpha_1(T)\mathbf{v}_0 e^{ik_c x} + \alpha^2(T)\mathbf{v}^{(1)} e^{2ik_c x} + |\alpha|^2 \mathbf{v}^{(2)} + \text{c.c.}, \quad (81)$$

with $\mathbf{v}^{(1)} = (v_1^{(1)}, v_2^{(1)})^T$, and $\mathbf{v}^{(2)} = (v_1^{(2)}, v_2^{(2)})^T$ satisfying the following two equations

$$L_{2k_c}(\mathbf{v}^{(1)}) + \mathbf{Q}^{(1)} = 0, \quad (82)$$

$$L_0(\mathbf{v}^{(2)}) + \mathbf{Q}^{(2)} = 0. \quad (83)$$

Solving system (82) gives us

$$v_1^{(1)} = \frac{-Q_1^{(1)}}{2\gamma ik + 2M_5 \hat{K}_2^+}, \quad v_2^{(1)} = v_1^{(1)}. \quad (84)$$

Here we define $\hat{K}_2^+ = q_r(\hat{K}_r^+(2k_c) - \hat{K}_r^-(2k_c)) - q_a^0(\hat{K}_a^+(2k_c) - \hat{K}_a^-(2k_c))$. System (83) reduces to one equation in two unknowns. To solve it for $v_1^{(2)}$ and $v_2^{(2)}$, we have to impose the conservation of the total density on the interval $[0, L] = [0, \frac{2\pi}{k_c}]$. This condition requires that $v_2^{(2)} = -v_1^{(2)}$. We therefore have

$$v_1^{(2)} = \frac{-Q_1^{(2)}}{2L_1}, \quad v_2^{(2)} = -v_1^{(2)}. \quad (85)$$

At $O(\epsilon^3)$, the nonlinear terms are given by

$$\mathbf{E}_3 = \left(\begin{array}{c} \frac{du_1^+}{dT} - (u^* + u^{**})P_1 v \left((\tilde{K}_a - K_a) * u_1 \right) \\ \frac{du_1^-}{dT} + (u^* + u^{**})P_1 v \left((\tilde{K}_a - K_a) * u_1 \right) \end{array} \right), \quad (86)$$

and

$$\mathbf{N}_3 = \left(\begin{array}{c} P_1(K * u_1)u_2 + P_1(K * u_2)u_1 + S_1(u_1^+ - u_1^-)(K * u_1)^2 + T_1 A(K * u_1)^3 \\ -P_1(K * u_1)u_2 - P_1(K * u_2)u_1 - S_1(u_1^+ - u_1^-)(K * u_1)^2 - T_1 A(K * u_1)^3 \end{array} \right), \quad (87)$$

where $u_1 = u_1^+ + u_1^-$, and $u_2 = u_2^+ + u_2^-$. At this step, secular terms can arise if $\mathbf{N}_3 + \mathbf{E}_3$ contains terms of the form $e^{\pm ik_c x}$. To eliminate these secular terms, we

impose the orthogonality condition (32). The solution \mathbf{W} of the adjoint equation (30) is given by

$$W_1 = 1, \quad W_2 = \frac{\gamma ik - L_1 - M_5 \hat{K}^-(k_c)}{-L_1 - M_5 \hat{K}^-(k_c)}. \tag{88}$$

Then, the orthogonality condition can be written as

$$\lim_{\hat{T} \rightarrow \infty} \frac{1}{\hat{T}} \int_0^{\hat{T}} \int_0^{\frac{2\pi}{k_c}} (\beta_1(T) \mathbf{W} e^{ik_c x} + \beta_2(T) \bar{\mathbf{W}} e^{-ik_c x}) \left(\mathbf{R}^{(1)} \alpha |\alpha|^2 e^{ik_c x} + \bar{\mathbf{R}}^{(1)} \bar{\alpha} |\alpha|^2 e^{-ik_c x} + \mathbf{R}^{(2)} \alpha e^{ik_c x} v + \bar{\mathbf{R}}^{(2)} \bar{\alpha} e^{-ik_c x} v + \mathbf{R}^{(3)} \frac{d\alpha}{dT} e^{ik_c x} + \bar{\mathbf{R}}^{(3)} \frac{d\bar{\alpha}}{dT} e^{-ik_c x} \right) dx dT = 0.$$

The coefficients $\mathbf{R}^{(j)}$, $j = 1, 2, 3$, are described by

$$\begin{aligned} R_1^{(1)} &= P_1 \bar{v} v^{(1)} \hat{K}^- + P_1 v v^{(2)} \hat{K}^+ + P_1 \bar{v} v^{(1)} \hat{K}_2^+ + S_1 (\bar{v}_1 - \bar{v}_2) v^2 (\hat{K}^+)^2 \\ &\quad + 2S_1 \bar{v} v (v_1 - v_2) \hat{K}^+ \hat{K}^- + 3T_1 A \bar{v} v^2 \hat{K}^- (\hat{K}^+)^2, \\ R_2^{(1)} &= -R_1^{(1)}, \\ R_1^{(2)} &= -M_5 v (\hat{K}_a^- - \hat{K}_a^+) (k_c), \\ R_2^{(2)} &= -R_1^{(2)}, \\ R_1^{(3)} &= v_1, \\ R_2^{(3)} &= v_2. \end{aligned} \tag{89}$$

We define here $v = v_1 + v_2$, and $v^{(1)} = v_1^{(1)} + v_2^{(1)}$. Since $\int_0^{\frac{2\pi}{k_c}} e^{\mp 2ik_c x} dx = 0$, we obtain

$$\bar{\mathbf{W}} \cdot \mathbf{R}^{(1)} \alpha |\alpha|^2 + \bar{\mathbf{W}} \cdot \mathbf{R}^{(2)} \alpha v + \bar{\mathbf{W}} \cdot \mathbf{R}^{(3)} \frac{d\alpha}{dT} = 0, \tag{90}$$

and its complex-conjugate

$$\mathbf{W} \cdot \bar{\mathbf{R}}^{(1)} \bar{\alpha} |\alpha|^2 + \mathbf{W} \cdot \bar{\mathbf{R}}^{(2)} \bar{\alpha} v + \mathbf{W} \cdot \bar{\mathbf{R}}^{(3)} \frac{d\bar{\alpha}}{dT} = 0. \tag{91}$$

Equation (90) can be rewritten as

$$\frac{1}{2} \frac{d\alpha}{dT} = -v Y \alpha - X \alpha |\alpha|^2, \tag{92}$$

with

$$X = \frac{\bar{\mathbf{W}} \cdot \mathbf{R}^{(1)}}{\bar{\mathbf{W}} \cdot \mathbf{R}^{(3)}} \quad Y = \frac{\bar{\mathbf{W}} \cdot \mathbf{R}^{(2)}}{\bar{\mathbf{W}} \cdot \mathbf{R}^{(3)}}. \quad (93)$$

The two steady-state solutions of this equation are $|\alpha|^2 = 0$ or $|\alpha|^2 = -\nu \frac{\Re(Y)}{\Re(X)}$ [see (39)]. To compare the results of the nonlinear analysis with the numerical results, we substitute α into the expressions for u_1^\pm and derive a formula for the actual amplitude of the spatial patterns:

$$\max(u) - \min(u) = \epsilon(\max(u_1^+ + u_1^-) - \min(u_1^+ + u_1^-)) = \epsilon 4\Re(\alpha(v_1 + v_2)). \quad (94)$$

Appendix 4: Detailed calculations for the weakly nonlinear analysis in the neighborhood of an imaginary bifurcation

The derivation of the amplitude equation for the case when the bifurcation of the unstable branch occurs through an imaginary eigenvalue follows the same steps as before. Here we consider only the case $q_r = q_a = 0$. The case when attraction and repulsion are nonzero is similar, but the equations are more complicated. At $O(\epsilon)$ we have

$$\mathbf{u}_1 = \alpha \mathbf{v} e^{i\omega t + ik_c x} + c.c. \quad (95)$$

where $\mathbf{u}_1 = (u_1^+, u_1^-)^T$, $\mathbf{v} = (v_1, v_2)^T$, and $\alpha = \alpha(T)$. At $O(\epsilon^2)$, $\mathbf{E}_2 = 0$ and

$$\mathbf{N}_2 = \begin{pmatrix} (u_1^+ P_1 + u_1^- P_2) q_{al}^0 K_{al} * (u_1^- - u_1^+) + (u^* S_1 - u^{**} S_2) (q_{al}^0)^2 (K_{al} * (u_1^- - u_1^+))^2 \\ -(u_1^+ P_1 + u_1^- P_2) q_{al}^0 K_{al} * (u_1^- - u_1^+) - (u^* S_1 - u^{**} S_2) (q_{al}^0)^2 (K_{al} * (u_1^- - u_1^+))^2 \end{pmatrix}.$$

After some calculations we can rewrite the nonlinear terms $\mathbf{N}_2 + \mathbf{E}_2$ as

$$\mathbf{N}_2 + \mathbf{E}_2 = \alpha^2 e^{2i\omega t + 2ik_c x} \mathbf{Q}^{(1)} + \bar{\alpha}^2 e^{-2i\omega t - 2ik_c x} \mathbf{Q}^{(2)} + |\alpha|^2 \mathbf{Q}^{(3)}. \quad (96)$$

Therefore, the solution of the nonlinear problem $L(\mathbf{u}_2) = \mathbf{N}_2 + \mathbf{E}_2$ can be written as

$$\mathbf{u}_2 = \alpha_1 \mathbf{v}_0 e^{i\omega t + ik_c x} + \alpha^2 e^{2i\omega t + 2ik_c x} \mathbf{G}_0^{(1)} + \bar{\alpha}^2 e^{-2i\omega t - 2ik_c x} \mathbf{G}_0^{(2)} + |\alpha|^2 \mathbf{G}_0^{(3)}.$$

The constants $\mathbf{G}_0^{(j)}$, $j = 1, 2, 3$, are calculated by requiring them to verify the following equations:

$$L_{2\omega, 2k_c} \mathbf{G}_0^{(1)} = -\mathbf{Q}^{(1)}, \quad L_{-2\omega, -2k_c} \mathbf{G}_0^{(2)} = -\mathbf{Q}^{(2)}, \quad L_{0,0} \mathbf{G}_0^{(3)} = -\mathbf{Q}^{(3)}. \quad (97)$$

The solution does not contain terms of the form $e^{\pm i\omega t \pm ik_c x}$ and therefore the Fredholm Alternative is satisfied. However, at $O(\epsilon^3)$ we have to impose the orthogonality condition $L^*(\hat{\mathbf{u}}) = 0$. Let us define the solution of the adjoint homogeneous problem to be

$\hat{\mathbf{u}} = \beta_1(T)\mathbf{V}e^{i\omega t + ik_c x} + c.c.$ Then, the orthogonality condition becomes $\bar{L}_{k_c}^T(\hat{\mathbf{u}}) = 0$, where

$$\bar{L}_{k_c}^T(\mathbf{u}) = \begin{pmatrix} -i\omega - \gamma ik_c + L_1 + M_5 q_{al}^0 K_{al}^+ & -L_1 - M_5 q_{al}^0 K_{al}^+ \\ -L_2 + M_5 q_{al}^0 K_{al}^- & -i\omega + \gamma ik_c + L_2 - M_5 q_{al}^0 K_{al}^- \end{pmatrix} \quad (98)$$

This leads to the amplitude equation (51), with the vector \mathbf{V} given by

$$V_1 = 1, \quad V_2 = \frac{i\omega + \gamma ik_c - L_1 + M_5 q_{al}^0 \hat{K}_{al}^+}{-L_1 + M_5 q_{al}^0 \hat{K}_{al}^+}. \quad (99)$$

At $O(\epsilon^3)$, we obtain the amplitude equation (51). The coefficients $\mathbf{R}^{(j)}$, $j = 1, 2, 3$, that appear in this equation are given by

$$\begin{aligned} R_1^{(1)} &= v_1, \\ R_2^{(1)} &= v_2, \\ R_1^{(2)} &= (M_5 + 2q_{al}^0(u^{**} - u^*)(u^* S_1 - u^{**} S_2))b_1 + (u^{**} - u^*)e_1 + 2q_{al}^0 e_1 + q_{al}^0 J_{11} b_1 \\ &\quad - q_{al}^0 (P_1 - P_2 - 4q_{al}^0 (u^* S_1 - u^{**} S_2) b_1), \\ R_2^{(2)} &= -R_1^{(2)}, \\ R_1^{(3)} &= 2(u^* S_1 - u^{**} S_2)(q_{al}^0)^2 (b_1 G_0^{(3)} + \bar{b}_1 G_0^{(1)}) + 3(u^* T_1 + u^{**} T_2)(q_{al}^0)^3 (b_1)^2 \bar{b}_1 \\ &\quad + q_{al}^0 (e_1 G_0^{(3)} + \bar{e}_1 G_0^{(1)}) + (q_{al}^0)^2 (\bar{f}_1 (b_1)^2 + 2f_1 b_1 \bar{b}_1) + q_{al}^0 (J_1 \bar{b}_1 + J_9 b_1), \\ R_2^{(3)} &= -R_1^{(3)}. \end{aligned} \quad (100)$$

We define here

$$\begin{aligned} b_1 &= \hat{K}_{al}^+ v_2 - \hat{K}_{al}^- v_1, \quad e_1 = P_1 v_1 + P_2 v_2, \quad f_1 = S_1 v_1 - S_2 v_2, \\ J_j &= G_1^{(j)} P_1 + G_2^{(j)} P_2, \quad j = 1 \dots 10, \\ G_0^{(1)} &= G_{0_2}^{(1)} \hat{K}_{al}^+(2k_c) - G_{0_1}^{(1)} \hat{K}_{al}^-(2k_c), \quad G_0^{(2)} = G_{0_2}^{(2)} \hat{K}_{al}^-(2k_c) - G_{0_1}^{(2)} \hat{K}_{al}^+(2k_c), \\ G_0^{(3)} &= G_{0_2}^{(3)} - G_{0_1}^{(3)}. \end{aligned} \quad (101)$$

References

1. Aldana M, Dossetti V, Huepe C, Kenke VM, Larralde H (2007) Phase transitions in systems of self-propelled agents and related network models. *Phys Rev Lett* 98(9):095,702

2. Beekman M, Sumpter DJT, Ratnieks FLW (2001) Phase transitions between disordered and ordered foraging in pharaoh's ants. *Proc Natl Acad Sci USA* 98(17):9703–9706
3. Bressloff PC (2004) Euclidean shift-twist symmetry in population models of self-aligning objects. *SIAM J Appl Math* 64:1668–1690
4. Bressloff PC, Cowan JD, Golubitsky M, Thomas PJ, Wiener MC (2001) Geometric visual hallucinations, euclidean symmetry and the functional architecture of striate cortex. *Phil Trans R Soc Lond B* 356:299–330
5. Buhl J, Sumpter DJT, Couzin ID, Hale JJ, Despland E, Miller ER, Simpson SJ (2006) From disorder to order in marching locusts. *Science* 312:1402–1406
6. Bullis HR (1961) Observations on the feeding behavior of white-tip sharks on schooling fishes. *Ecology* 42:194–195
7. Chaté H, Ginelli F, Grégoire G (2007) Comment on “phase transitions in systems of self-propelled agents and related network models”. *Phys Rev Lett* 99:229,601
8. Couillet P, Ioos G (1990) Instabilities of one-dimensional cellular patterns. *Phys Rev Lett* 64(8): 866–869
9. Couzin ID, Krause J, James R, Ruxton G, Franks NR (2002) Collective memory and spatial sorting in animal groups. *J Theor Biol* 218:1–11
10. Cross MC, Hohenberg PC (1993) Pattern formation outside equilibrium. *Rev Mod Phys* 65(3): 851–1112
11. Czirók A, Barabási AL, Vicsek T (1999) Collective motion of self-propelled particles: kinetic phase transition in one dimension. *Phys Rev Lett* 82(1):209–212
12. Czirók A, Stanley H, Vicsek T (1997) Spontaneously ordered motion of self-propelled particles. *J Phys A Math Gen* 30:1375–1385
13. Eftimie R, de Vries G, Lewis MA (2007) Complex spatial group patterns result from different animal communication mechanisms. *Proc Natl Acad Sci USA* 104(17):6974–6979
14. Eftimie R, de Vries G, Lewis MA, Lutscher F (2007) Modeling group formation and activity patterns in self-organizing collectives of individuals. *Bull Math Biol* 69(5):1537–1566
15. Flierl G, Grünbaum D, Levin S, Olson D (1999) From individuals to aggregations: the interplay between behavior and physics. *J Theor Biol* 196:397–454
16. Gazi V, Passino KM (2002) Stability analysis of swarms. In: *Proceedings of American control conference on Anchorage, AK*, pp 8–10
17. Golubitsky M, Stewart I, Schaeffer DG (1988) *Singularities and groups in bifurcation theory, vol II*. Springer, Heidelberg
18. Grégoire G, Chaté H (2004) Onset of collective and cohesive motion. *Phys Rev Lett* 92(2):025,702
19. Gueron S, Levin SA, Rubenstein DI (1996) The dynamics of herds: from individuals to aggregations. *J Theor Biol* 182:85–98
20. Helbing D, Treiber M (1999) Numerical simulations of macroscopic traffic equations. *Comput Sci Eng* 1(5):89–98
21. Hillen T (1995) Nichtlineare hyperbolische systeme zur modellierung von ausbreitungsvorgängen und anwendung auf das turing modell. PhD Thesis, Universität Tübingen
22. Hillen T, Stevens A (2000) Hyperbolic models for chemotaxis in 1-D. *Nonlinear Anal Real World Appl* 1:409–433
23. Huth A, Wissel C (1994) The simulation of fish schools in comparison with experimental data. *Ecol Model* 75/76:135–145
24. Keener J (1988) *Principles of applied mathematics*. Addison-Wesley, Reading
25. Lutscher F (2002) Modeling alignment and movement of animals and cells. *J Math Biol* 45:234–260
26. Lutscher F, Stevens A (2002) Emerging patterns in a hyperbolic model for locally interacting cell systems. *J Nonlinear Sci* 12:619–640
27. Mallet-Paret J (1999) The fredholm alternative for functional differential equations of mixed type. *J Dyn Differ Equ* 11(1):1–47
28. Matkowski BJ (1970) Nonlinear dynamic stability. *SIAM J Appl Math* 18:872–883
29. Mirabet V, Auger P, Lett C (2007) Spatial structures in simulations of animal grouping. *Ecol Model* 201:468–476
30. Mogilner A, Edelstein-Keshet L (1996) Spatio-angular order in populations of self-aligning objects: formation of oriented patches. *Physica D* 89:346–367
31. Mogilner A, Edelstein-Keshet L (1999) A non-local model for a swarm. *J Math Biol* 38:534–570
32. Murray JD (1984) *Asymptotic analysis*. Springer, Heidelberg

33. Newell AC, Passot T, Lega J (1993) Order parameter equations for patterns. *Annu Rev Fluid Mech* 25:399–453
34. Niwa HS (1994) Self-organizing dynamical model of fish schooling. *J Theor Biol* 171:123–136
35. Okubo A, Grünbaum D, Edelstein-Keshet L (2001) The dynamics of animal grouping. In: Okubo A, Levin S (eds) *Diffusion and ecological problems: modern perspectives*. Springer, New York, pp 197–237
36. Othmer HG, Dunbar SR, Alt W (1988) Models of dispersal in biological systems. *J Math Biol* 26: 263–298
37. Pfisterer B (1990) A one dimensional model for the swarming behavior of Myxobacteria. In: Alt W, Hoffmann G (eds) *Biological motion, Lecture Notes on Biomathematics*, vol 89. Springer, Heidelberg, pp 556–563
38. Pfisterer B, Alt W (1990) A two dimensional random walk model for swarming behavior. In: Alt W, Hoffmann G (eds) *Biological motion, Lecture Notes on Biomathematics*, vol 89. Springer, Heidelberg, pp 564–565
39. Reuter H, Breckling B (1994) Self organization of fish schools: an object-oriented model. *Ecol Model* 75(76):147–159
40. Reynolds CW (1987) Flocks, herds and schools: a distributed behavioral model. *Comput Graph* 21: 25–34
41. Robinson JC (2001) *Infinite-dimensional dynamical systems*. Cambridge University Press, Cambridge
42. Springer S (1966) Some observations of the behavior of schools of fishes in the gulf of mexico and adjacent waters. *Ecology* 38:166–171
43. Stuart JT (1960) On the nonlinear mechanism of wave disturbances in stable and unstable parallel flows. part I. *J Fluid Mech* 9:353–370
44. Topaz CM, Bertozzi AL (2004) Swarming patterns in a two-dimensional kinematic model for biological groups. *SIAM J Appl Math* 65:152–174
45. Topaz CM, Bertozzi AL, Lewis MA (2006) A nonlocal continuum model for biological aggregation. *Bull Math Biol* 68:1601–1623
46. Vabø R, Nøttestad L (1997) An individual based model of fish school reactions: predicting antipredator behaviour as observed in nature. *Fish Oceanogr* 6:155–171
47. Vicsek T, Czirók A, Ben-Jacob E, Cohen I, Shochet O (1995) Novel type of phase transition in a system of self-driven particles. *Phys Rev Lett* 75(6):1226–1229